Journal of Physiology (1988), **400**, *pp.* 237–274
With 15 *text-figures*
Printed in Great Britain

KINETIC ANALYSIS OF VOLTAGE- AND ION-DEPENDENT CONDUCTANCES IN SACCULAR HAIR CELLS OF THE BULL-FROG, *RANA CATESBEIANA*

BY A. J. HUDSPETH AND R. S. LEWIS

From the Department of Physiology, University of California School of Medicine, San Francisco, CA 94143-0444, U.S.A.

(*Received 23 March 1987*)

SUMMARY

1. By the use of whole-cell and excised-patch tight-seal recording techniques, we studied ionic conductances in voltage-clamped solitary hair cells isolated from the bull-frog's sacculus. As a basis for assessing their contributions to hair cell electrical resonance, we developed kinetic models describing voltage-dependent Ca^{2+} and Ca^{2+}-dependent K^+ conductances.

2. A transient K^+ current (I_A) was activated by steps to potentials positive to -50 mV from holding potentials more negative than -70 mV. In the steady state, the current was fully inactivated at the normal resting potential. Possibly due to the dissipation of a Donnan potential between the pipette's interior and the cell, the voltage dependence of I_A inactivation slowly shifted in the negative direction during whole-cell recording.

3. The voltage-gated Ca^{2+} current (I_{Ca}) was isolated by blocking I_A with 4-aminopyridine (4-AP) and Ca^{2+}-activated K^+ current with tetraethylammonium (TEA). The I_{Ca} was activated at potentials more positive than -60 to -50 mV and was maximal at about -10 mV. Its magnitude was highly variable among cells, with an average value of -240 pA at -30 mV. Its activation could be fitted well by a third-order (m^3) gating scheme.

4. A Ca^{2+}-activated K^+ current ($I_{K(Ca)}$) was isolated as the component of membrane current blocked by TEA. This current was activated at potentials more positive than -60 to -50 mV and had an average value of 1·5 nA at -30 mV. The Ca^{2+}-activated K^+ conductance ($g_{K(Ca)}$) showed a high apparent voltage dependence, increasing e-fold every 3 mV at potentials between -50 and -40 mV.

5. The Ca^{2+}-activated K^+ current displayed rapid activation and deactivation kinetics. The current reached half-maximal activation in 2–4 ms at voltages between -50 and -30 mV, and the tail current decayed exponentially with a time constant of 1·0 ms at -70 mV. The activation rate and magnitude of $I_{K(Ca)}$ were reduced by lowering the extracellular Ca^{2+} concentration.

6. The open probability of Ca^{2+}-activated K^+ channels was estimated by ensemble-fluctuation analysis of whole-cell currents evoked by voltage steps to -30 mV. The average open probability was estimated to be 0·8 at this potential.

7. K^+-selective channels with a high conductance (140–200 pS) were examined in

excised, inside-out membrane patches. The activity of these channels depended on intracellular Ca^{2+} and membrane potential. These properties suggest that the channels underlie the whole-cell Ca^{2+}-activated K^+ current.

8. Open- and closed-lifetime histograms of single Ca^{2+}-activated K^+ channels under steady-state conditions of intracellular Ca^{2+} concentration and membrane potential suggest that the channel has at least two open and three closed states. Based on these results, a five-state, linear kinetic scheme was adopted in which two Ca^{2+} ions bind to open the channel, and a third Ca^{2+} ion can bind to prolong the opening.

9. Depolarizing voltage pulses opened Ca^{2+}-activated K^+ channels in the presence of a constant intracellular Ca^{2+} concentration. Channels opened with a sigmoidal time course and closed rapidly upon repolarization.

10. We developed a model linking intracellular Ca^{2+} accumulation and membrane potential to activation of K^+ channels. According to this formulation, Ca^{2+} ions enter the cell through Ca^{2+} channels whose opening is described by a third-order kinetic scheme. The incoming Ca^{2+} accumulates in a submembrane compartment, in which it can activate K^+ channels according to a five-state kinetic scheme. The removal of Ca^{2+} from the submembrane compartment is a first-order process.

11. Parameter values in the model were chosen to produce accurate fits of a series of Ca^{2+} currents and Ca^{2+}-activated K^+ currents recorded in one cell at potentials of -55 to -30 mV. Thus constrained, the model can account for the effects of reducing the extracellular Ca^{2+} concentration on $I_{K(Ca)}$. By this test, the model is a reasonable description of the activation of $I_{K(Ca)}$ in the intact cell.

INTRODUCTION

The hair cells of the vertebrate inner ear transduce stimuli derived from sound or acceleration into receptor potentials. In some cases, the responses of hair cells are made selective for stimuli of particular frequencies through a tuning mechanisms based upon electrical resonance in their membranes (Crawford & Fettiplace, 1980, 1981; Ashmore, 1983; Lewis & Hudspeth, 1983*a*). Their responses are transmitted to the auditory or vestibular nerve across chemical synapses that not only forward information about the steady-state membrane potential (Sewell, 1984), but also respond rapidly enough to convey information about the phase of receptor potentials up to frequencies of at least 9 kHz (Sullivan & Konishi, 1984).

These functions of transduction, tuning, and synaptic transmission are mediated to a large extent through the activity of ion channels (for a review, see Hudspeth, 1986). The transduction channel, a mechanically gated, non-selective cation channel associated with the hair bundle, has been extensively characterized (for reviews, see Hudspeth, 1983, 1985). The present paper and its companion (Hudspeth & Lewis, 1988) deal instead with the voltage- and ion-dependent channels responsible for three membrane conductances: a voltage-dependent Ca^{2+} conductance (g_{Ca}), a transient, voltage-dependent, A-type K^+ conductance (g_A), and a Ca^{2+}-sensitive K^+ conductance ($g_{K(Ca)}$). Two of these conductances, g_{Ca} and $g_{K(Ca)}$, effect electrical resonance, while g_{Ca} is likely in addition to mediate the release of synaptic transmitter. All three types of channels were first studied in hair cells using tight-seal

recording techniques on cells dissociated from the bull-frog's sacculus (Lewis & Hudspeth, 1983*b*). In this paper we further characterize the kinetic properties and voltage and ion sensitivities of these three conductances, primarily in the potential range in which the cells display electrical resonance. Based upon the experimental results, we develop a quantitative model that links changes in intracellular Ca^{2+} concentration ($[Ca^{2+}]_i$), resulting from ion flux through Ca^{2+} channels, to control of the Ca^{2+}-activated K^+ conductance. This model is used in the companion paper to establish the sufficiency of these conductances to account for electrical resonance (Hudspeth & Lewis, 1988). Preliminary reports of this work have been presented (Lewis, 1984*a*, *b*; Hudspeth, 1985, 1986).

METHODS

Dissociation of hair cells

Sacculi were dissected from adult bull-frogs (*Rana catesbeiana*) and treated for 25 min at 20–22 °C with papain (Calbiochem, San Diego, CA; 300–500 mg l^{-1}) dissolved in oxygenated saline solution containing 120 mM-Na^+, 2 mM-K^+, 100 μM-Ca^{2+}, 2·5 mM-L-cysteine, 130 mM-Cl^-, 3 mM-D-glucose, and 5 mM-HEPES (pH 7·2). Following this treatment, each sacculus was placed in a similar oxygenated saline in which bovine serum albumin (500 mg l^{-1}) replaced the papain and cysteine. After 30–60 min, hair cells were dissociated from the sacculus by gently scraping the macular epithelium with a sharpened tungsten needle, after which they settled on, but did not adhere to, the glass bottom of the recording chamber. Although papain from other suppliers (Worthington Biochemical Products and Sigma Chemical Co.) expressed higher levels of papain activity as assayed by hydrolysis of benzoylarginine ethyl ester, it was ineffective in loosening hair cells from the epithelium at comparable concentrations. This result suggests that a contaminating enzyme in Calbiochem papain is the active dissociating agent.

Whole-cell recording

Experiments were conducted on the fixed stage of a microscope (WL, Carl Zeiss, Oberkochen, F.R.G.) equipped with a 40×, water-immersion objective lens and differential-interference-contrast optics. Solitary hair cells were voltage or current clamped following methods described by Hamill, Marty, Neher, Sakmann & Sigworth (1981), using a whole-cell clamp based on the Mark V design of the Yale Physiology Department Electronics Shop (New Haven, CT). Recording pipettes were fabricated from soda-lime-glass capillaries (Kimble R-6, Garner Glass Co., Claremont, CA) coated near their tips with silicone plastic (Sylgard 184, Dow Corning Corp., Midland, MI) and heat-polished to internal tip diameters of 2–3 μm. The pipettes were filled with internal solutions whose compositions are listed in Table 1 and had axial resistances of 1–3 MΩ. Unless otherwise indicated, recordings were made from cells bathed in standard saline using pipettes that were filled with K^+–aspartate internal solution. A chlorided silver wire connected the pipette interior with the input of the headstage, which incorporated an amplifier (OPA101, Burr-Brown, Tucson, AZ) with a 200-MΩ feed-back resistance. The frequency response of the recording system was essentially flat up to 4 kHz. After formation of a tight seal between a pipette and cell, the residual capacitance of the pipette was nulled electronically. Slight suction was then applied to the pipette to rupture the patch of membrane under the pipette and produce the whole-cell recording configuration.

Solution changes. In general, the Ca^{2+} and Ca^{2+}-activated K^+ conductances in solitary hair cells began to decline after several minutes of whole-cell recording. To expedite voltage- and current-clamp measurements in different external solutions while the conductances were stable, we moved the cell (or membrane patch, in single-channel experiments) sequentially into continously flowing streams of test solutions (Lewis & Hudspeth, 1983*b*). The solutions (Table 1) were pumped into the recording chamber at a rate of 2 μl s^{-1} by a peristaltic pump (Minipuls 2, Gilson, Villiers-le-Bel, France) and were removed by a siphon.

Series-resistance compensation. The series resistance, (R_s) between the headstage input and the cell's membrane, was assessed by analysing the response to a 10 mV voltage pulse (ΔV_m) that elicited only passive leakage and capacitive currents. The capacitive transient at the start of the

TABLE 1. Composition of solutions. V_{JP} denotes the junction potential between the listed solution and standard saline. The pH of all solutions is 7·2

External saline solutions

Solution	Na^+ (mM)	K^+ (mM)	Ca^{2+} (mM)	Mg^{2+} (mM)	TEA (mM)	4-AP (mM)	Cl^- (mM)	Glucose (mM)	HEPES (mM)	V_{JP} (mV)
Standard saline	120	2	4	—	—	—	128	3	5	0
TEA saline	100	2	4	—	20	—	128	3	5	0
4-AP saline	110	2	4	—	—	10	128	3	5	0
TEA–4-AP saline	90	2	4	—	20	10	128	3	5	1
Low-Ca^{2+} saline	120	2	0·5	3·5	—	—	128	3	5	0
1 mM-TEA saline	119	2	4	—	1	—	128	3	5	0
KCl saline	—	122	4	—	—	—	128	3	5	−4

Internal solutions

Solution	K^+ (mM)	Cs^+ (mM)	Na^+ (mM)	Ca^{2+} (mM)	Mg^{2+} (mM)	Asp (mM)	Cl^- (mM)	EGTA (mM)	Glucose (mM)	HEPES (mM)	V_{JP} (mV)
K^+–aspartate	124	—	—	0·134	2	120	4.3	2	3	5	−13
Cs^+–aspartate	—	124	—	0·134	2	120	4.3	2	3	5	−3
KF	126	—	—	0·002	2	—	4·0	2	3	5	9
KCl											
+ 1 μM-Ca^{2+}	122	—	3	0·875	2	—	128	1	3	5	−4
+ 10 μM-Ca^{2+}	122	—	3	0·010	2	—	127	—	3	5	−4
+ 100 μM-Ca^{2+}	122	—	3	0·100	2	—	127	—	3	5	−4
K^+–aspartate											
+ 1 μM-Ca^{2+}	127	—	—	2·00	2	120	8	2	3	5	−13
+ 8 μM-Ca^{2+}	128	—	—	2·32	2	120	8·6	2	3	5	−13
+ 26 μM-Ca^{2+}	128	—	—	2·40	2	120	8.8	2	3	5	−13
+ 100 μM-Ca^{2+}	128	—	—	2·71	2	120	9·4	2	3	5	−13
+ 167 μM-Ca^{2+}	128	—	—	3·00	2	120	10	2	3	5	−13

pulse was integrated to give the total charge displacement (Q) and the membrane capacitance was calculated as $C_m = Q/\Delta V_m$. The decay of the transient was fitted with an exponential function that was filtered by the time constant of the clamp circuit (about 40 μs). The value of R_s was then calculated from the relation $\tau = R_s C_m$, in which τ is the time constant of decay of the capacitive transient; R_s ranged from 2 to 6 MΩ, with an average value of 4·4 MΩ ($n = 35$). We used an average of 50% series-resistance compensation, leading to membrane-potential errors of less than 3 mV during the ionic currents of less than 1 nA that were typical in the experiments reported here. Somewhat larger voltage errors would be expected during the larger capacitive currents elicited at the start and end of voltage pulses. In most cases, however, this was not a significant problem: the membrane potential exponentially approached the command potential level with a time constant of about 30 μs, as calculated by the product of C_m and the uncompensated R_s. Constant suction of 2–4 kPa (200–400 mmH_2O) was applied to most cells during whole-cell recordings to prevent slow increases in R_s.

Liquid-junction potentials

Immediately before formation of the tight seal, a small potential was applied to the pipette to bring its current to zero. K^+–aspartate, KF and KCl solutions produced significant liquid-junction potentials with respect to standard saline (Table 1). These values were added to or subtracted from applied command potentials to calculate actual potentials respectively in whole-cell and inside-out-patch voltage-clamp experiments. In current-clamp experiments, junction-potential values were added to the apparent pipette potential to obtain the true membrane potential.

Stimulation and recording

Command potentials and currents were generated by a 12-bit digital-to-analog converter (AD566J, Analog Devices, Norwood, MA) in a computer interface (Cheshire Data, New Haven, CT). Stimuli were controlled by a PDP-11/23 computer (Digital Equipment Corporation, Maynard, MA) using stimulation and recording programs written in BASIC-23 (Indec Systems, Sunnyvale, CA). Data were sampled synchronously with a 12-bit analog-to-digital converter (DT2768, Data Translation, Marlboro, MA).

Current or voltage pulses were applied sequentially from the most negative to the most positive values, at repetition intervals of 500–1000 ms, unless otherwise noted. In voltage-clamp experiments, linear leakage and capacitive currents were removed by subtracting multiples of the average response to eight small (−10 or −20 mV) voltage pulses given immediately prior to each family of test-potential pulses.

Ensemble-variance analysis

Ensemble-variance analysis of macroscopic Ca^{2+}-activated K^+ currents was performed by the procedure of Sigworth (1980). We assume that the cell has a homogeneous population of Ca^{2+}-activated K^+ channels that exhibit only one non-zero conductance level and are gated independently of each other. When such a cell is stimulated repeatedly, the following relations hold:

$$I = Nip, \tag{1}$$

and

$$\sigma^2 = Ni^2p(1-p), \tag{2}$$

in which I is the mean macroscopic current, N is the total number of channels that can be activated, i is the single-channel current amplitude, p is the open-state probability, and σ^2 is the current's variance. The parameters I, p, and σ^2 are functions of time. Equation (2) predicts that the fluctuations in current resulting from the stochastic gating of ion channels approach zero when none or all of the channels are activated ($p = 0$ or $p = 1$), and are largest when half are open ($p = 0{\cdot}5$). Equations (1) and (2) can be combined to yield a parabolic relation between current variance and mean current,

$$\sigma^2 = iI - I^2/N. \tag{3}$$

Leakage current was recorded as the average response to a set of sixteen pulses of +10 or −20 mV amplitude, delivered respectively from a holding potential of −70 or −55 mV. The Ca^{2+}-activated K^+ current ($I_{K(Ca)}$) was next elicited by a group of eight pulses to −30 mV. Each group of eight responses was corrected using the preceding leakage current, then averaged to give the local mean current. Local variance around the mean was calculated by squaring the difference

between each of the eight individual responses and the local mean current, then averaging the results. Grand averages were made from the local means and variances throughout the recording period until the local mean $I_{K(Ca)}$ had deteriorated by more than 10% from its starting value. The contribution of Ca^{2+} current (I_{Ca}) to the total current was cancelled by subtracting from the grand-average current an appropriately scaled, third-order waveform (Hodgkin & Huxley, 1952) with a time constant of 400 μs, which corresponds to the average kinetic behaviour of I_{Ca} in hair cells at this potential (Lewis & Hudspeth, 1983*b*; Roberts, Robles & Hudspath, 1986). The grand average for variance was plotted point-for-point against that of the corrected grand-average current, and a parabola described by eqn (3) was fitted to the plot using a least-square-error criterion.

Single-channel recording

The activity of single Ca^{2+}-activated K^+ channels was recorded from excised, inside-out membrane patches (Hamill *et al.* 1981). Borosilicate glass pipettes (50 μl Microcaps, Drummond Scientific Co., Broomall, PA) were coated with silicone plastic, then heat-polished to give resistances of 5–10 MΩ when filled with standard saline. After a tight seal formed between the pipette and the cell's membrane, the micromanipulator (Ernst Leitz, Wetzlar, F.R.G.) was tapped sharply to excise a membrane patch. The solution facing the intracellular side of the patch was controlled by placing the pipette's tip in a stream of internal solution, and liquid-junction potentials of the pipette and external perfusion solutions relative to the bath were corrected as described above. The output of the amplifier (EPC-5, List Electronik, Darmstadt, F.R.G.) was low-pass filtered with an eight-pole Bessel filter (902LPF, Frequency Devices, Inc., Haverhill, MA). Unless stated otherwise, the filter's cut-off frequency was 2 kHz and data were sampled at 100 μs intervals. Calcium chloride was added to internal solutions containing EGTA to provide the desired levels of free Ca^{2+}; the effective dissociation constant for Ca^{2+} was 146 nM at pH 7·20 as measured by the method of Bers (1982). Final adjustments of the free Ca^{2+} concentration were made using a calibrated Ca^{2+} electrode (93–20, Orion Research, Cambridge, MA).

Data for histogram analysis were recorded on an FM tape recorder (3968A, Hewlett-Packard, San Diego, CA) having a passband of 0–5 kHz. For computer analysis, these data were replayed and digitally sampled at a frequency five times the Bessel filter's cut-off frequency of 2 kHz. The amplitudes of single-channel currents were estimated either by fitting amplitude histograms of sampled data with a Gaussian curve, or, if satisfactory histograms were not obtainable, by visually fitting lines to 'square' current events.

For the construction of channel-lifetime histograms, data were digitized as described above and interpolated using a cubic-spline algorithm (Colquhoun & Sigworth, 1983), resulting in an interpoint time interval of 25 μs. After the baseline current was fitted by eye, opening and closing transitions were detected using a threshold criterion of 50% of the open-channel current magnitude. Short events were corrected for the rise time of the recording apparatus (Colquhoun & Sigworth, 1983). Single- or double-exponential conditional-probability-density functions of the form

$$f(t) = \frac{\sum_i (a_i/\tau_i) \exp(-t/\tau_i)}{P(t > t_{min})}, \tag{4}$$

were fitted to the data; $f(t)$ is the probability density of an event of duration t given that it is longer than the minimum detectable duration (t_{min}) and a_i is the area and τ_i the time constant of the ith exponential component of the probability-density function. The parameter $P(t > t_{min})$ is the probability that the event is longer than t_{min}. A maximum-likelihood method (Colquhoun & Sigworth, 1983) was used to fit the probability-density function to the data.

The current–voltage relation for open Ca^{2+}-activated K^+ channels was obtained by the ramp-clamp method (Yellen, 1982). Repetitive voltage ramps were applied to a patch; open- and closed-channel segments of the data were identified off-line and averaged separately, point-by-point for each potential. The closed-channel average was subtracted from the open average to give the net current–voltage relation for the single open channel.

Voltage-dependent relaxations of the Ca^{2+}-activated K^+ channel's open-state probability were also studied in the presence of constant concentrations of Ca^{2+} on the intracellular membrane surface. Repetitive voltage pulses were applied to the patch and closed-channel segments identified and averaged as in ramp-clamp experiments. The closed-channel average, comprising a small leakage current and residual capacitive transients, was subtracted from the average of all responses.

Modelling the Ca^{2+}-activated K^+ current

A model presented in the text describes the activation of $I_{K(Ca)}$ in terms of Ca^{2+}-current activation, the resultant accumulation of Ca^{2+} inside the cell, and Ca^{2+}-dependent activation of K^+ channels. The equations pertaining to these three parts of the model are presented in the Appendix, which also details the reasoning employed in the selection of numerical values for the model's parameters.

RESULTS

Whole-cell recording from solitary hair cells

Electrical resonance and ionic currents. Electrical resonance is manifested in hair cells as damped membrane-potential oscillations elicited by the injection of current pulses (Crawford & Fettiplace, 1981; Ashmore, 1983; Lewis & Hudspeth, 1983*b*). A response of this sort is illustrated in Fig. 1*A*, in which a solitary hair cell was stimulated with a 375 pA pulse of current. Resonant behaviour under current-clamp conditions was observed at membrane potentials ranging from the resting potential (−60 to −50 mV) to about −30 mV. To investigate the ionic basis of the resonance phenomenon, we voltage-clamped solitary hair cells to potentials in this same range. As depicted in Fig. 1*B*, a voltage-clamp pulse from −70 to −40 mV, corresponding to the peak of the potential oscillation in Fig. 1*A*, elicited a complex current that we have identified as the combination of an early, inward current carried by Ca^{2+} ions through voltage-dependent, non-inactivating Ca^{2+} channels (I_{Ca}), followed by outward current carried by K^+ ions through Ca^{2+}-activated K^+ channels ($I_{K(Ca)}$) (Lewis & Hudspeth, 1983*a*). An additional, voltage-dependent, transient K^+ current (A-current; I_A) is not apparent in this experiment because of its inactivation at the holding potential (see below).

Separation of ionic currents under voltage-clamp conditions. Because the magnitudes of the conductances g_{Ca}, $g_{K(Ca)}$ and g_A varied considerably from cell to cell, any attempt to relate them to the generation of electrical resonance, or to link voltage-dependent Ca^{2+} influx to activation of $g_{K(Ca)}$, required methods of separating the three ionic currents so that each could be studied independently in an individual cell. These methods are illustrated in Fig. 2.

The A-current was isolated using its property of voltage-dependent inactivation (Connor & Stevens, 1971; Neher, 1971; Lewis & Hudspeth, 1983*b*). Depolarizing the hair cell's membrane from a holding potential of −100 to +25 mV elicits outward Ca^{2+}-activated K^+ and A-currents (Fig. 2*A*, upper trace). Depolarization to the same level from a more positive holding potential of −60 mV, at which I_A is completely inactivated in the steady state, activates only an outward $I_{K(Ca)}$ (Fig. 2*A*, middle trace). Point-by-point subtraction of the second current record from the first thus isolates I_A (Fig. 2*A*, right trace).

The A-current in hair cells is blocked completely and specifically by 10 mM-4-aminopyridine (4-AP; Lewis & Hudspeth, 1983*b*). With the A-current eliminated by this means, the specific sensitivity of $I_{K(Ca)}$ to tetraethylammonium ion (TEA) can be used to separate I_{Ca} and $I_{K(Ca)}$ (Lewis & Hudspeth, 1983*b*). The upper trace in Fig. 2*B* shows a combination of inward Ca^{2+} current and outward Ca^{2+}-activated K^+ current elicited by depolarization to −30 mV. With 20 mM-TEA added exter-

nally to block $I_{K(Ca)}$, the same depolarization evokes only I_{Ca} (Fig. 2*B*, lower trace). Subtraction of the second response from the first removes the contribution of I_{Ca} to the total current, leaving $I_{K(Ca)}$ (Fig. 2*B*, right trace). This procedure allowed us to measure I_{Ca} and $I_{K(Ca)}$ in the same cell, as was necessary to derive a quantitative description of $I_{K(Ca)}$ activation in terms of channel-mediated Ca^{2+} influx.

Transient K^+ current (A-current). Depolarizing the hair cell's membrane to potentials more positive than −50 mV from holding potentials more negative than

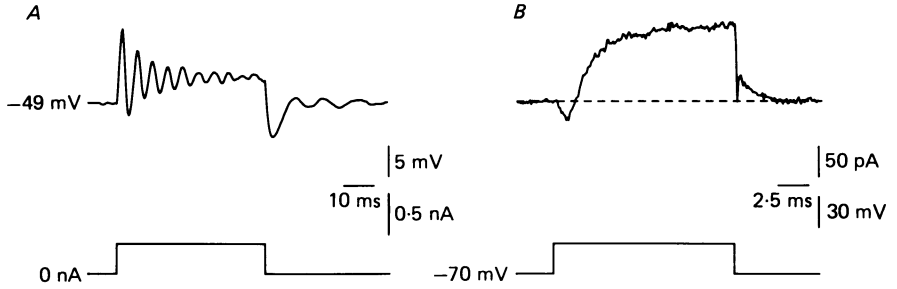

Fig. 1. Electrical resonance and ionic currents in solitary hair cells. *A*, oscillation in membrane potential (top trace) produced by a 375 pA pulse of depolarizing current (bottom trace). Resting potential: −49 mV. Cell 60; average of three responses. *B*, ionic current evoked by voltage-clamp depolarization. The magnitude of the voltage pulse (from −70 to −40 mV, bottom trace) corresponds to the potential range in which the cell in *A* is electrically resonant. The evoked current (upper trace) is a combination of rapid inward Ca^{2+} current followed by outward Ca^{2+}-activated K^+ current. Cell 36.

−70 mV elicits a transient, outward K^+ current, which we have classified as an A-current (Lewis & Hudspeth, 1983*b*) based on its kinetic and pharmacological similarities to I_A in molluscan neurones (Connor & Stevens, 1971; Neher, 1971). A series of A-currents, isolated by the subtraction method outlined above, is illustrated in Fig. 3*A*. The voltage dependence of I_A activation is shown by a plot of peak current against potential (Fig. 3*B*). A conspicuous feature of the A-current, and one that is crucial for assessing its role in generating membrane phenomena such as electrical resonance, is its voltage-dependent inactivation. Inactivation of A-channels during prolonged depolarization leads to a decrease in the outward K^+ current with time (Fig. 3*A*). The voltage dependence of inactivation was assessed by holding the membrane at different potentials until in each case a steady level of inactivation was attained; the peak I_A evoked by subsequent depolarization to a fixed level of −20 mV was employed to indicate the fraction of non-inactivated channels. The results of this experiment, illustrated in Fig. 4, show that the cell must be hyperpolarized to membrane potentials more negative than −70 mV before a significant number of A-channels become available for activation; a potential of −100 mV or below is required to remove inactivation fully (Fig. 4*B*). This result, which was confirmed in fifteen additional cells, implies that under the conditions employed in current-clamp experiments (e.g. Fig. 1*A*), in which the membrane is depolarized from a resting value in the range of −50 to −60 mV, g_A is fully inactivated and therefore does not contribute to electrical resonance.

In many of the experiments dealing with the A-current, we used an internal

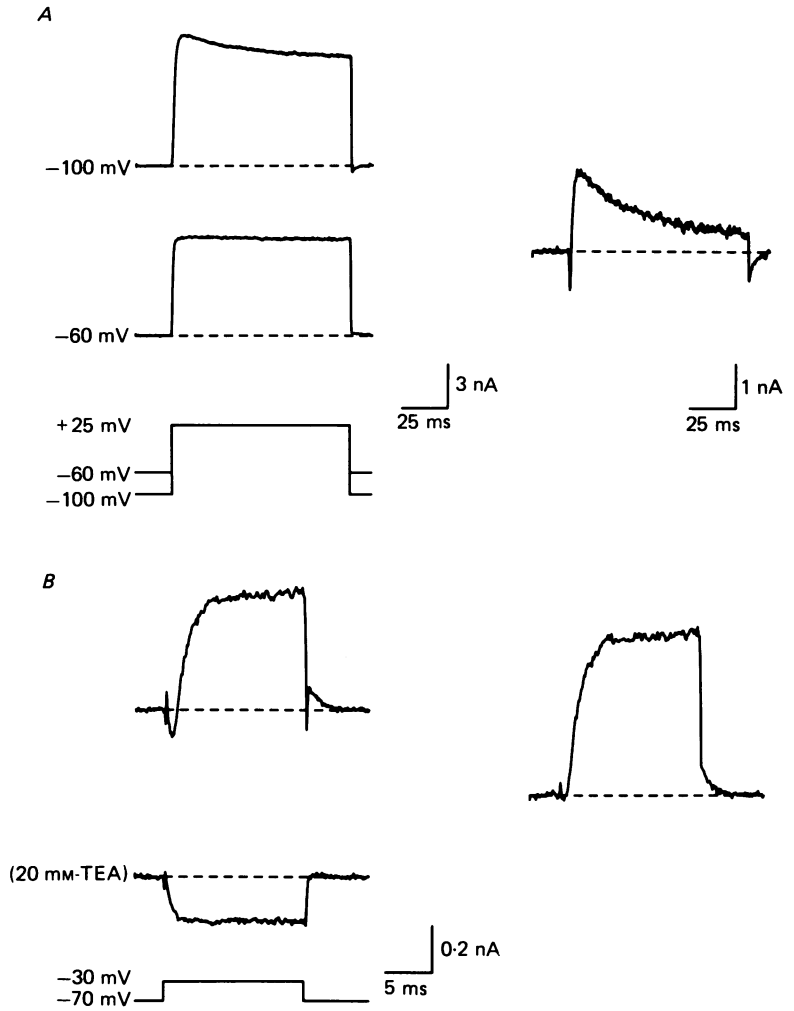

Fig. 2. Separation of A-current, Ca^{2+} current and Ca^{2+}-activated K^+ current. *A*, isolation of transient K^+ current (A-current). In standard saline, membrane depolarization from −100 to 25 mV (bottom left) activates a combination of I_{Ca}, $I_{K(Ca)}$, and I_A (top left). Depolarization to the same value from a holding potential of −60 mV, at which I_A is inactivated, elicits only I_{Ca} and $I_{K(Ca)}$ (middle left). Subtraction of the second response from the first isolates I_A, which is shown at higher gain to the right. Cell 23*i*. *B*, measurement of Ca^{2+} and Ca^{2+}-activated K^+ currents from a single cell. With I_A blocked by 10 mM-4-AP, depolarization from −70 to −30 mV elicits I_{Ca} followed by $I_{K(Ca)}$ (upper left). Addition of 20 mM-TEA blocks $I_{K(Ca)}$, so that the same depolarization evokes only I_{Ca} (middle left). Subtraction of the current in the presence of TEA from that in its absence isolates $I_{K(Ca)}$, as shown to the right. Cell 36.

solution containing fluoride as the major anion; this procedure maintained I_A for more than 30 min. During such extended recordings, we observed a slow shift of −10 to −15 mV in the voltage dependence of steady-state I_A inactivation (Fig. 4*C*). The fact that a parallel shift occurred concomitantly in the voltage dependence of I_A activation suggests that the membrane potential was slowly becoming more positive.

A shift similar to that described here has been observed during whole-cell recordings of Na^+ currents in other cell types (Marty & Neher, 1983; Fernandez, Fox & Krasne, 1984) and has been attributed to the slow dissipation of a Donnan potential across the tip of the recording pipette. According to this hypothesis, the presence of large, relatively immobile intracellular anions makes the true membrane potential 10–15 mV more negative than the command potential at early times after establishing the whole-cell configuration. As these cellular anions slowly equilibrate across the tip of

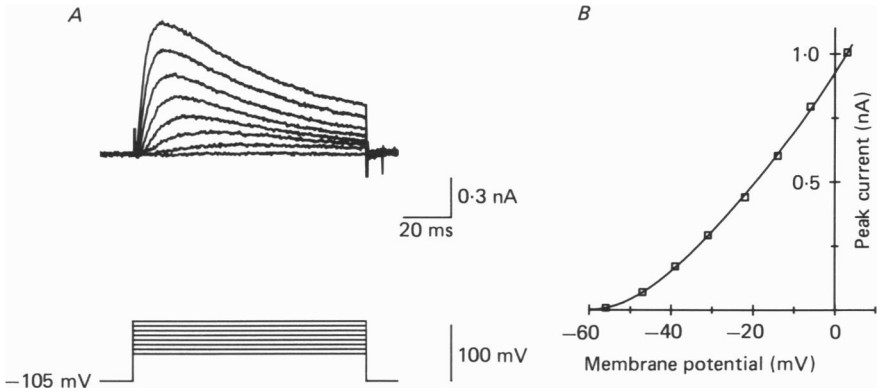

Fig. 3. Activation of the transient K^+ current (A-current). *A*, I_A (upper traces) evoked by depolarizing voltage pulses to levels from −56 to +3 mV (lower traces). The currents were isolated by the subtraction method described in Fig. 2*A*, using holding potentials of −65 and −105 mV. *B*, peak I_A (from *A*) plotted against the membrane potential during the pulse. The A-current in hair cells is activated at potentials more positive than about −50 mV. Cell 13*i*.

the recording pipette, the associated junction potential dissipates, and membrane potential approaches the command potential.

Calcium conductance in solitary hair cells. The majority of hair cells that we studied in detail (twenty-four of twenty-six cells) displayed a voltage-dependent Ca^{2+} conductance which was activated at potentials more positive than −60 to −50 mV (Lewis & Hudspeth, 1983*b*). Its magnitude was quite variable among experiments; as measured shortly after the start of recording, the steady-state I_{Ca} at −30 mV ranged from 0 to −650 pA with a mean of −240 pA. Because cells dissociated from a given sacculus tended to have relatively uniform Ca^{2+} conductances, the differences in g_{Ca} among different experiments may have been due to varying amounts of damage caused by the cell-dissociation procedure, rather than to natural variation. In addition, the Ca^{2+} current deteriorated irreversibly during the course of whole-cell recording from single cells. To avoid artifacts related to Ca^{2+}-current run-down, we analysed only those data collected during the first few minutes after establishment of the whole-cell recording configuration, before the Ca^{2+} current had declined significantly.

Figure 5*A* shows a series of Ca^{2+} currents evoked by depolarization to potentials of −50 to +10 mV. In this cell, I_{Ca} is activated at potentials positive to −50 mV and attains a maximum at −10 mV (Fig. 5*B*). To estimate the proportion of Ca^{2+} channels open at each voltage in the steady state, we measured Ca^{2+} tail currents at

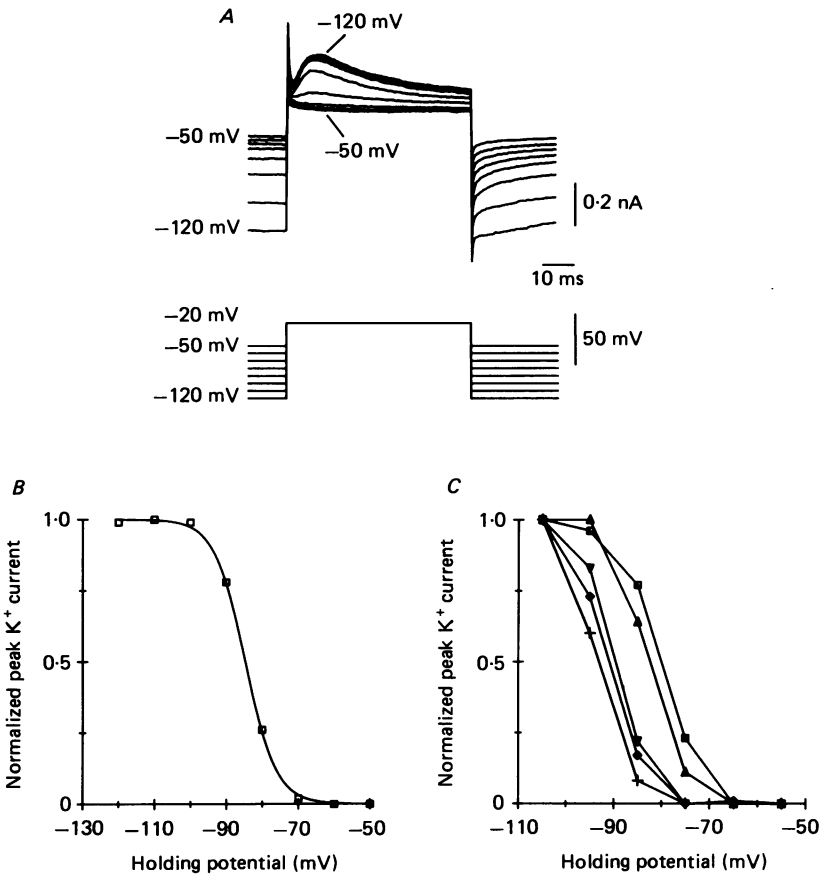

Fig. 4. Voltage-dependent inactivation of the A-current. *A*, I_A, without correction for leakage or capacitive current, evoked by voltage pulses to −20 mV delivered from holding potentials of −120 to −50 mV (lower traces). Data were recorded starting 12·5 min after establishing the whole-cell recording configuration, with 2 s between stimuli to allow I_A inactivation to reach a steady value at each holding potential. The largest A-current, showing the least amount of steady-state inactivation, corresponds to the most negative holding potential. Cell 92; internal solution, KF. *B*, steady-state inactivation of I_A as a function of holding potential (data from *A*). The extent of inactivation was estimated by the ratio of I_A evoked from a given holding potential to that elicited from a holding potential of −100 mV. The data were fitted with a Boltzmann curve of the form $I = I_{max}/\{1+\exp[(V_m - V_{\frac{1}{2}})/\kappa]\}$, in which I is the current at a given membrane potential, I_{max} is the peak current, V_m is membrane potential, $V_{\frac{1}{2}}$ is the potential at which half the channels are inactivated, and κ is a factor describing the voltage sensitivity of inactivation. For the curve shown, $V_{\frac{1}{2}} = 84{\cdot}5$ mV and $\kappa = 4{\cdot}3$ mV. *C*, slow shift in the voltage dependence of I_A inactivation during the course of whole-cell recording. Steady-state inactivation is plotted as a function of holding potential for various times after the start of whole-cell recording: □, 0·75 min, △, 2·7 min; ▽, 11·9 min; ◇, 15·3 min; +, 24·5 min. Over a period of about 30 min, $V_{\frac{1}{2}}$ shifted from −80 to −93 mV. Cell 73; internal solution, KF.

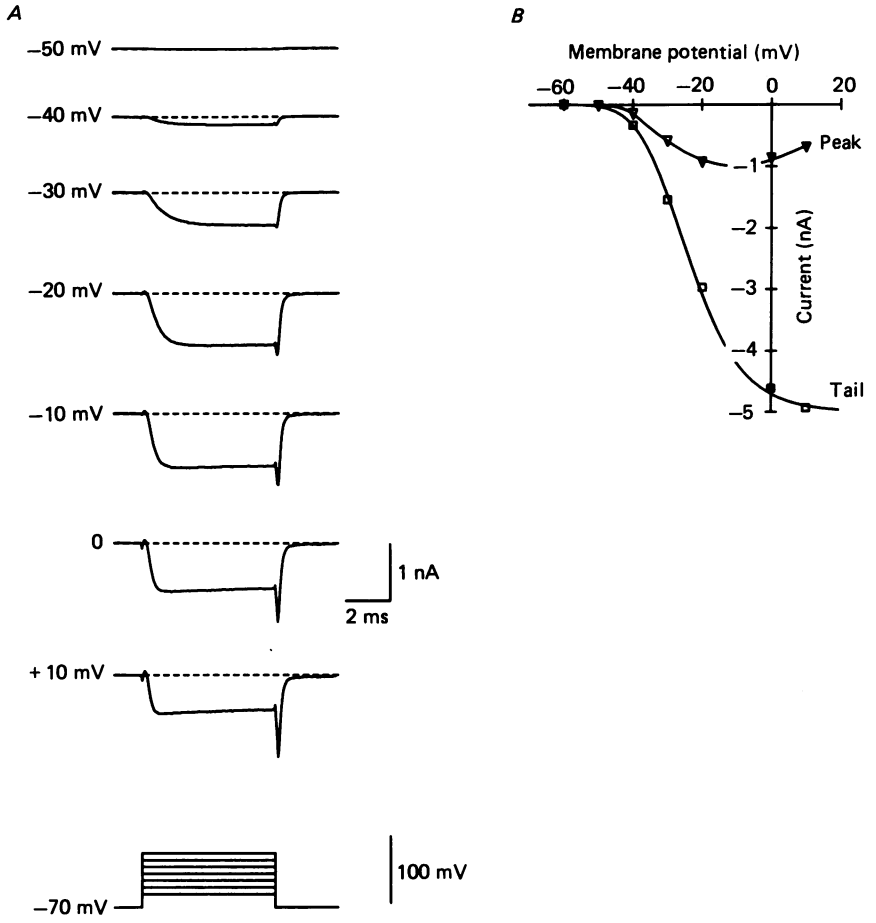

Fig. 5. Voltage dependence of Ca^{2+}-current activation. *A*, I_{Ca} evoked by a series of depolarizations from a holding potential of −70 mV to the values indicated to the left of each trace. Cell 50; internal solution, Cs^+–aspartate. *B*, peak Ca^{2+} current and initial magnitude of Ca^{2+} tail current (from *A*) as a function of the pulse potential. Tail-current amplitudes were estimated from single-exponential extrapolations back to the end of the pulse. A Boltzmann relation of the form $I = I_{max}/\{1+\exp[-(V_m - V_{\frac{1}{2}})/\kappa]\}^3$ has been fitted to the tail-current data by a least-square-error criterion; I is the peak amplitude of the tail current at a given membrane potential, I_{max} is the peak tail current with all Ca^{2+} channels open, V_m is the command voltage during the pulse, $V_{\frac{1}{2}}$ is the potential at which the steady-state activation parameter, m_∞, takes on a value of 0·5, and κ is a slope factor describing the voltage dependence of activation. For the curve shown, $I_{max} = -5{\cdot}0$ nA, $V_{\frac{1}{2}} = -36{\cdot}5$ mV, and $\kappa = 9{\cdot}4$ mV. g_{Ca} in this cell, as measured from tail-current magnitudes, was half-maximal at −24 mV.

the holding potential immediately following each pulse. The peak magnitude of the Ca^{2+} tail current increased with depolarization, approaching a maximum value following pulses to +10 mV (Fig. 5*B*). On the assumption that the maximum tail current ensues from the opening of all the Ca^{2+} channels, these results suggest that the Ca^{2+} conductance is fully activated above this potential.

Kinetic description of the whole-cell Ca^{2+} current. We studied the activation of the

Ca^{2+} current in greatest detail at membrane potentials between −50 and −30 mV. Figure 6*A* shows a series of Ca^{2+} currents evoked by voltage pulses in this range. The activation time course of this current is adequately described by a third-order kinetic scheme without inactivation (Hodgkin & Huxley, 1952; Lewis & Hudspeth, 1983*b*; Ohmori, 1984),

$$I_{Ca} = \bar{g}_{Ca} m^3 (V_m - E_{Ca}), \tag{5}$$

in which $\bar{g}_{Ca}$ is the limiting value of Ca^{2+} conductance when all Ca^{2+} channels are open, m is the value of the time- and voltage-dependent activation parameter, and E_{Ca} is the Ca^{2+} equilibrium potential. Following a step change in potential, the activation parameter, m, varies with time according to the relation

$$m(t) = m_0 + (m_\infty - m_0)[1 - \exp(-t/\tau_m)], \tag{6}$$

in which m_0 is the value of m before the potential change and τ_m is the time constant of m's exponential approach to m_∞, its equilibrium value at the new potential. Further details of this kinetic scheme are discussed in the Appendix.

The predictions of the model, seen superimposed on the data traces in Fig. 6*A*, were generated in the following way. First, the results of the Ca^{2+} tail-current experiments (Fig. 5) provided an estimate of 42±6% activation at −30 mV (four cells), or $m_\infty^3 = 0{\cdot}42$. This value was substituted for the m^3 term in eqn (5) to estimate the cell's limiting Ca^{2+} conductance, $\bar{g}_{Ca}$, on the assumption that $E_{Ca} = 100$ mV. Values for m_∞ and τ_m (Fig. 6*C*) were then chosen to generate best fits to the observed I_{Ca} waveform at each potential. These values were used to calculate α_m and β_m, the opening and closing rate constants for the m gate (Appendix, eqns (9) and (10)). Finally, exponential fits to plots of α_m and β_m against voltage (Fig. 6*D*) provided the empirical relations (Appendix, eqns (11) and (12)) that were employed to produce the model waveforms shown in Fig. 6*A*.

Kinetic description of Ca^{2+}-activated K^+ current in whole-cell recordings. In over 95% of the cells studied, depolarization to potentials more positive than −60 to −50 mV activated a Ca^{2+}-dependent K^+ current (Lewis & Hudspeth, 1983*b*). In fifty-six cells, the steady-state $I_{K(Ca)}$ measured at −30 mV ranged from 0·3 to 3·9 nA with a mean of 1·5 nA. Figure 7*A* shows a series of Ca^{2+}-activated K^+ currents, recorded from the same cell as that used for Fig. 6. As might be expected from its dependence on intracellular Ca^{2+}, $I_{K(Ca)}$ showed approximately the same voltage threshold for activation as I_{Ca} (compare Figs 7*B* and 6*B*).

Tail-current analysis revealed that activation of $I_{K(Ca)}$ was highly voltage dependent. The fit of a Boltzmann relation to the tail-current amplitudes in Fig. 7*B* indicates an e-fold increase in conductance for every 3 mV depolarization at potentials between −50 and −40 mV. As will be shown below, the apparent voltage dependence of $I_{K(Ca)}$ activation in the hair cell has two sources. First, the opening of Ca^{2+}-activated K^+ channels is dependent on the internal Ca^{2+} concentration ($[Ca^{2+}]_i$); $I_{K(Ca)}$ thus derives much of its voltage dependence indirectly from the voltage dependence of Ca^{2+} channels. In addition, the gating of Ca^{2+}-activated K^+ channels is to some extent intrinsically voltage dependent.

The time course of activation if $I_{K(Ca)}$ is complex and cannot be approximated well by a Hodgkin–Huxley kinetic scheme (Hodgkin & Huxley, 1952) of any order (Lewis & Hudspeth, 1983*b*). The current is characterized by a relatively long delay followed

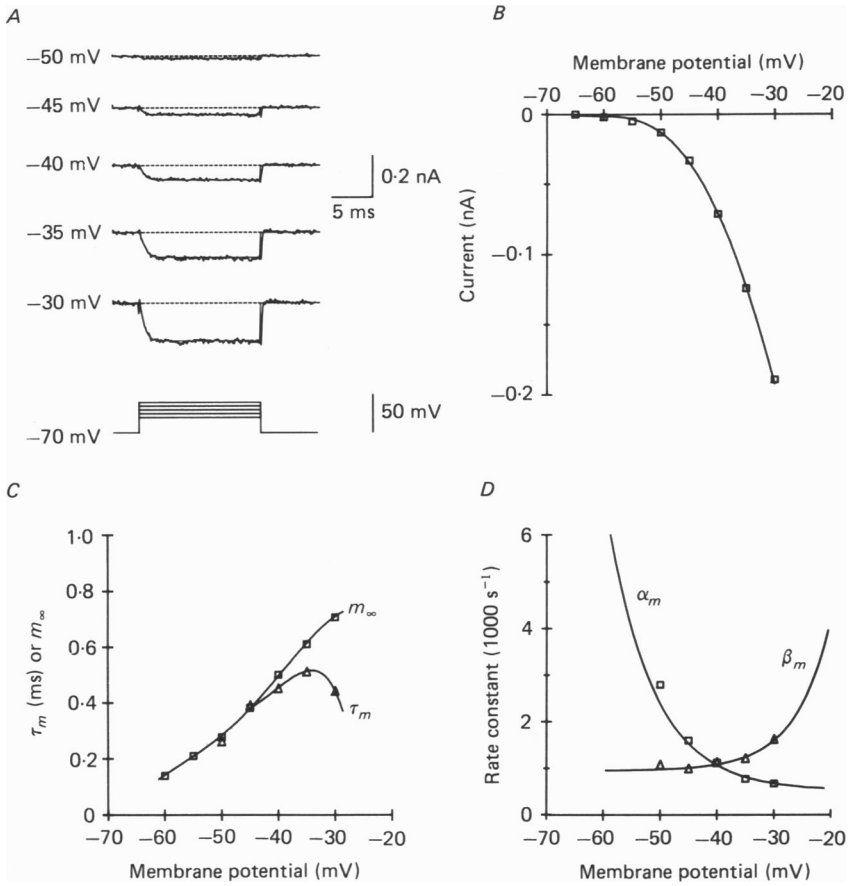

Fig. 6. Kinetic analysis of the Ca^{2+} current. *A*, inward Ca^{2+} currents (upper traces) evoked by depolarizations to values indicated to the left of each trace, delivered from a holding potential of −70 mV. Superimposed on each data trace is the current predicted by a third-order kinetic scheme without inactivation, using the parameter values listed in Table 2. Cell 36; external solution, TEA–4-AP saline. *B*, steady-state current–voltage relation for the Ca^{2+} current. The steady-state values of I_{Ca} from *A*, which are plotted against command potential, show significant activation at potentials positive to −60 mV. *C*, voltage dependence of the steady-state activation parameter, m_∞, and time constant, τ_m, of the kinetic scheme fitted to the data in *A*. *D*, voltage dependence of the opening (β_m) and closing (α_m) Ca^{2+}-channel rate constants. These values were derived from m_∞, and τ_m using eqns (9) and (10). An exponential curve of the form $\beta_m = \beta_0 \exp[(V_m + V_0)/V_B] + K_B$ was fitted by eye to the β_m points, with $\beta_0 = 0{\cdot}97\ s^{-1}$, $V_0 = 70$ mV, $V_B = 6{\cdot}2$ mV, and $K_B = 940\ s^{-1}$. An exponential function of the form $\alpha_m = \alpha_0 \exp[-(V_m + V_0)/V_A] + K_A$ was fitted to the α_m points, with $\alpha_0 = 22800\ s^{-1}$, $V_0 = 70$ mV, $V_A = 8{\cdot}0$ mV, and $K_A = 510\ s^{-1}$.

by a rapid rate of activation. The difference in the activation rates of I_{Ca} and $I_{K(Ca)}$ is illustrated in Fig. 7*C*, in which the early phases of the two currents from Figs 6*A* and 7*A* have been plotted together on an expanded time scale. For each of the voltage steps, I_{Ca} developed first, following a delay of only 200–300 μs. The latencies for activation of $I_{K(Ca)}$ were about 3-fold longer, ranging from 1·2 ms at −50 mV to 0·8 ms at −30 mV. Following its relatively slow onset, $I_{K(Ca)}$ was activated rapidly,

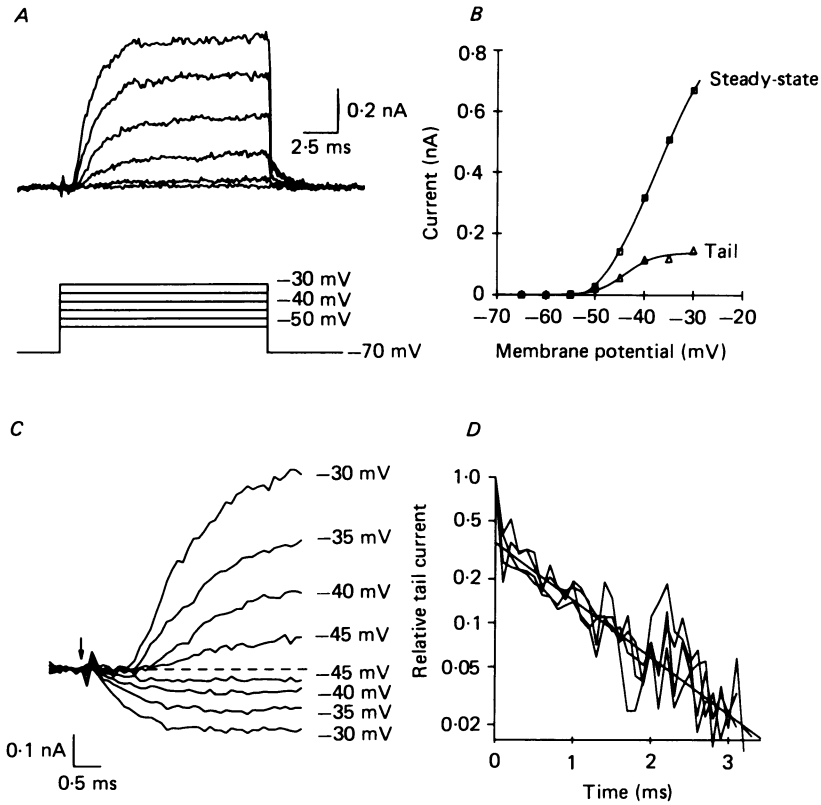

Fig. 7. Time courses of activation and deactivation of the Ca^{2+}-activated K^+ current. *A*, $I_{K(Ca)}$ (upper traces) elicited by a series of depolarizations (lower traces), as isolated by the TEA-subtraction protocol described in Fig. 2*B*. Cell 36. *B*, steady-state and peak tail $I_{K(Ca)}$ from *A*, plotted against the command potential. $I_{K(Ca)}$ in this cell was activated at potentials positive to −55 mV. Peak tail current was estimated by exponential extrapolation of the tail current back to the end of the pulse. A Boltzmann curve of the form $I = I_{max}/\{1+\exp[-(V_m - V_{\frac{1}{2}})/\kappa]\}$ has been fitted by eye to the tail current data; I_{max} is the maximum tail current, V_m is command voltage during the pulse, $V_{\frac{1}{2}}$ is the voltage eliciting half-maximal tail current, and κ is a constant denoting the apparent voltage dependence of activation. For the curve shown, $I_{max} = 0{\cdot}14$ nA, $V_{\frac{1}{2}} = -44$ mV, and $\kappa = 2{\cdot}8$ mV. This fit indicates an e-fold rise in conductance for 3 mV depolarization between −50 and −40 mV. *C*, comparison of the activation rates of outward $I_{K(Ca)}$ (from *A*) and inward I_{Ca} (from Fig. 6) in the same cell, shown on an expanded time scale. Command potentials are indicated to the right of each trace. Both currents commence along a sigmoidal time course, but the latency between the start of the voltage pulse (indicated by the arrow) and measurable ionic current is considerably longer for $I_{K(Ca)}$ than for I_{Ca}. *D*, amplitudes of K^+ tail currents following the voltage pulses in *A* plotted on a logarithmic scale relative to the initial value of each tail current, as a function of time. $I_{K(Ca)}$ decays as a single exponential with a time constant of 1·0 ms (straight line) irrespective of the size of the activating pulse.

reaching half of its steady-state magnitude in only 2–4 ms at potentials between −50 and −30 mV. Upon repolarization to −70 mV, tail currents decayed exponentially with a time constant of $1{\cdot}0 \pm 0{\cdot}3$ ms (S.D., $n = 18$ cells) that was independent of the size of the preceding depolarization (Fig. 7*D*).

In an effort to understand the factors contributing to the rapid activation of $I_{K(Ca)}$

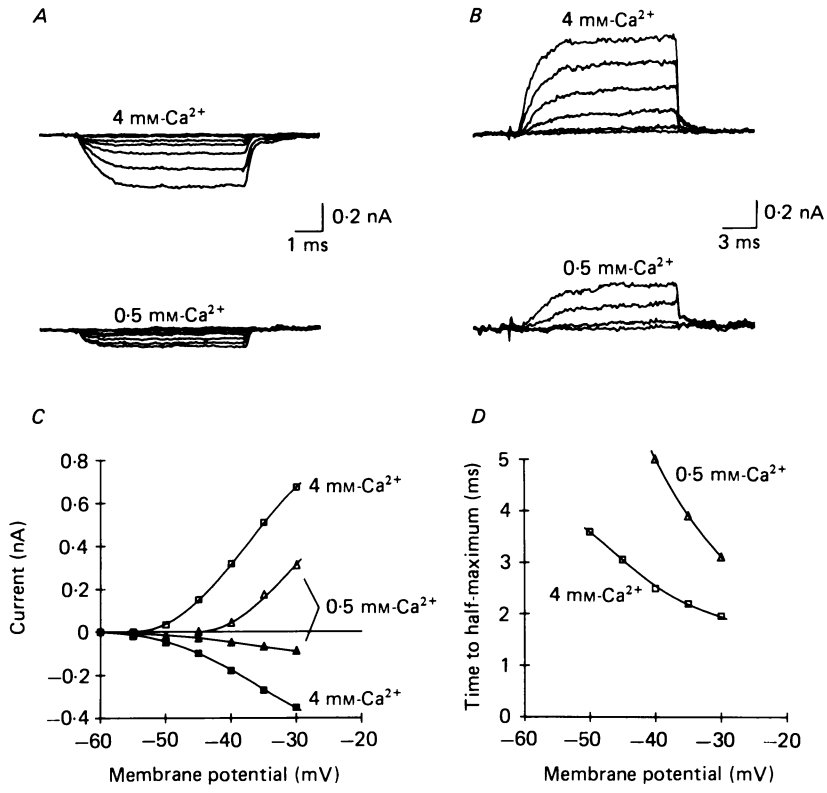

Fig. 8. Ca^{2+} dependence of I_{Ca} and $I_{K(Ca)}$. *A*, Ca^{2+} currents evoked by a series of voltage-clamp pulses from −60 to −30 mV in 5 mV increments, delivered from a holding potential of −70 mV. The currents were recorded in the presence of 4 mM-Ca^{2+} (top traces) or 0·5 mM-Ca^{2+} and 3·5 mM-Mg^{2+} (lower traces). The largest current in each case was elicited by the pulse to −30 mV. Cell 51; internal solution, Cs^+–aspartate. *B*, Ca^{2+}–activated K^+ currents evoked by voltage pulses from −55 to −30 mV (4 mM-Ca^{2+}) or from −45 to −30 mV (0·5 mM-Ca^{2+}), delivered in 5 mV increments from a holding potential of −70 mV. Cell 36. *C*, current–voltage relations for outward $I_{K(Ca)}$ and inward I_{Ca} at two external Ca^{2+} concentrations (data from *A* and *B*). Both currents are diminished by lowering $[Ca^{2+}]_o$, a treatment that also shifts the activation-potential 'threshold' for $I_{K(Ca)}$ towards more positive voltages. *D*, rate of $I_{K(Ca)}$ activation as a function of voltage and $[Ca^{2+}]_o$ (data from *B*). Activation rate is expressed as the time for $I_{K(Ca)}$ to attain half its steady-state value at each potential. Lowering $[Ca^{2+}]_o$ from 4 to 0·5 mM retards the activation of $I_{K(Ca)}$, presumably due to the reduced rate of Ca^{2+} entry into the cell.

in the hair cell, we studied the dependence of its activation rate and magnitude on the extracellular Ca^{2+} concentration. Complete removal of external Ca^{2+}, with or without substitution by Mg^{2+}, abolishes both I_{Ca} and $I_{K(Ca)}$ (Lewis & Hudspeth, 1983*b*). However, less drastic reduction of external Ca^{2+}, from 4 to 0·5 mM, lowers I_{Ca} at all potentials by about 75% (Fig. 8*A*) and reduces the rate of activation and the steady-state magnitude of $I_{K(Ca)}$ (Fig. 8*B*). The effects of Ca^{2+} influx on $I_{K(Ca)}$ are most extreme at potentials that activate a small fraction of the K^+ channels, and diminish with depolarization (Fig. 8*C* and *D*).

Several arguments suggest that the effects on $I_{K(Ca)}$ of reducing extracellular Ca^{2+} are due to a reduced influx of Ca^{2+} rather than to an effect on the membrane's surface potential. First, screening of the extracellular surface charge was kept constant by substituting Mg^{2+} for Ca^{2+}. Because Ca^{2+} generally binds somewhat more effectively to membrane sites than does Mg^{2+}, this substitution may locally depolarize the membrane by several millivolts at these sites (Hille, Woodhall & Shapiro, 1975). This effect may contribute to the slightly faster activation of I_{Ca} we have observed in 0·5 mM-external Ca^{2+}. Such a shift in surface potential is, however, in the wrong direction to explain the observed decrease in $I_{K(Ca)}$. Furthermore, reducing the influx of Ca^{2+} by partially blocking I_{Ca} with 20–50 μM-Cd^{2+} produced similar effects on $I_{K(Ca)}$. Taken together, these results suggest that the rate of Ca^{2+} influx through Ca^{2+} channels is a major determinant of the activation rate and magnitude of $I_{K(Ca)}$ in hair cells.

The dependence of $I_{K(Ca)}$ magnitude on Ca^{2+} influx is easily explained; lowering the rate of Ca^{2+} entry produces a smaller increase in the level of internal Ca^{2+} and hence opens a smaller number of Ca^{2+}-activated K^+ channels. The observed decrease in the activation rate of $I_{K(Ca)}$ could arise from at least two sources. First, the opening of Ca^{2+}-activated K^+ channels by internal Ca^{2+} may be co-operative, in that more than one Ca^{2+} ion must bind to open the channel. In addition, the transition rates between states of the Ca^{2+}-activated K^+ channel may be functions of $[Ca^{2+}]_i$. The results of single-channel experiments in other preparations (Magleby & Pallotta, 1983; Moczydlowski & Latorre, 1983; Pallotta, Hepler, Oglesby & Harden, 1987) and in hair cells (data presented below) support both of these hypotheses.

To understand more fully the relation between Ca^{2+} influx and the consequent opening of Ca^{2+}-activated K^+ channels, it is important to know the proportion of the cell's K^+ channels that is opened during a voltage-clamp pulse. The fraction of open K^+ channels may be estimated from tail-current amplitudes. As illustrated in Fig. 7*B*, the initial magnitude of Ca^{2+}-activated K^+ tail current appears to reach a maximal value following voltage pulses approaching −30 mV. This result could indicate that nearly all of the cell's Ca^{2+}-activated K^+ channels are open at this potential in the steady state. This would be an overestimate, however, if intracellular $[Ca^{2+}]$ reaches a maximum at potentials approaching −30 mV that is insufficient to activate $g_{K(Ca)}$ fully.

To estimate more directly the fraction of open Ca^{2+}-activated K^+ channels, we applied the method of ensemble-variance analysis (Sigworth, 1980) to measurements of whole-cell $I_{K(Ca)}$. Repetitive voltage-clamp pulses to −30 mV were used to activate $I_{K(Ca)}$; the results of four such presentations from one cell are illustrated in Fig. 9*A*. Subtraction of the mean of eight such responses from these records isolates the fluctuations in $I_{K(Ca)}$ around the mean, which are shown at higher gain in Fig. 9*B*. The large increase in current noise during the voltage pulse is presumably caused by the independent, stochastic activity of many Ca^{2+}-activated K^+ channels. Figure 9*C* shows the mean current and variance for thirty-two depolarizations of this cell. The variance reached a maximum during the rising phase of the mean current. Since the variance should be greatest when half of the channels are open on average, this result indicates that most of the cell's Ca^{2+}-activated K^+ channels were open at −30 mV in the steady state. The variance also increased slowly during the later part of the

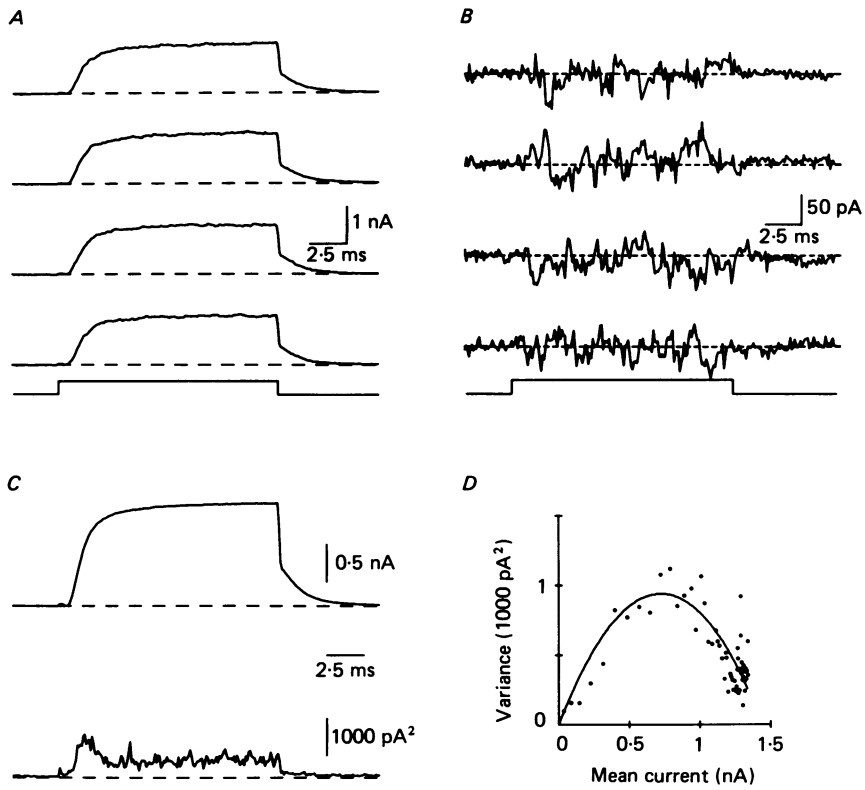

Fig. 9. Ensemble-fluctuation analysis of the whole-cell Ca^{2+}-activated K^+ current. *A*, $I_{K(Ca)}$ evoked by four consecutive voltage-clamp pulses to −30 mV delivered from a holding potential of −55 mV. The stimulus time course is shown at the bottom. Cell 46. *B*, stochastic current fluctuations obtained by subtracting the mean of eight current responses from each trace in *A*. *C*, mean of thirty-two $I_{K(Ca)}$ responses (top) and the corresponding average current variance (bottom), derived from the square of current fluctuations about the mean. The small initial rise in macroscopic current and variance marks the start of the voltage-clamp pulse. A slowly rising component of the fluctuations, evident during the later part of the pulse, may have been caused by a contaminating outward current. *D*, current variance plotted against mean current. This is a point-by-point plot of the lower trace against the upper trace of *C*. The slowly rising component of variance in the latter two-thirds of the response has been excluded. A parabolic fit to the points (eqn (3)) with a least-squares method is consistent with a single-channel current amplitude of 2·6 pA and a total of 550 Ca^{2+}-activated K^+ channels in the cell, with an open-state probability at −30 mV of 0·96 in the steady state.

pulse; this may have been caused by summation of a slowly activating current with $I_{K(Ca)}$. The slowly rising component of the variance was not included in the analysis. The total number of Ca^{2+}-activated K^+ channels in the cell and the amplitude of the single-channel (or elementary) current underlying the macroscopic current were estimated by fitting a parabola (eqn (3)) to a plot of variance against mean current (Fig. 9*D*). In this case, the fit indicated that the cell had 550 Ca^{2+}-activated K^+ channels, each producing an elementary current of 2·6 pA at −30 mV. The probability of a channel being open, as calculated from the number of channels, the

size of the elementary current, and the magnitude of the macroscopic current (eqn (1)), was 0·96 at −30 mV. For fifteen cells tested at −30 mV, the number of Ca^{2+}-activated K^+ channels per cell was 1493 ± 1108 (S.D.), the open-state probability in the steady state was 0·82 ± 0·11 (S.D.), and the single-channel current was 1·83 ± 0·49 pA (S.D.).

Single-channel recordings from excised membrane patches

Identification of Ca^{2+}-activated K^+ channels in excised patches. Over half of the inside-out patches we excised from the basolateral membrane surfaces of hair cells contained high-conductance, K^+-selective ion channels whose activity was modulated by both $[Ca^{2+}]_i$ and membrane potential. The slope conductance of these channels was determined from the amplitudes of single-channel currents at different holding potentials. An example of this experiment, in which the channel was activated by 100 μM-Ca^{2+} contacting the intracellular face of the membrane, is shown in Fig. 10*A*. The channel had a slope conductance of 195 pS measured between −50 and +40 mV; the reversal potential of 1·3 mV was close to the value of 0 mV that would be expected from the equal concentrations of KCl on both sides of the membrane in this experiment (Fig. 10*C*). The unitary conductance and reversal potential were unaffected by changes in $[Ca^{2+}]_i$ over the range of 1–100 μM. In experiments on twelve patches, with 122 mM-K^+ on both sides of the membrane or with 122 mM-K^+ on one side and standard saline (containing 2 mM-K^+) on the other, single-channel conductances ranged from 120 to 240 pS with an average of 154 pS. This large range of conductances may betray the presence of multiple types of Ca^{2+}-activated K^+ channels, as has been reported for mammalian outer hair cells (Ashmore & Meech, 1986). The large single-channel conductance we observe here resembles that of 'maxi' Ca^{2+}-activated K^+ (or BK) channels in a variety of preparations (for a review, see Latorre & Miller, 1983).

Measurements of the reversal potential for single-channel currents under different ionic conditions show that the channel is selectively permeable to K^+ over Cl^- and Na^+. With KCl saline and K^+–aspartate plus 100 μM-Ca^{2+} solutions (Table 1) bathing respectively the extracellular and intracellular faces of the membrane, the current through the channel reversed at 0·8 ± 1·2 mV (S.D., $n = 3$). Because aspartate is generally less permeant than Cl^- through Cl^- channels, a significant Cl^- permeability would produce a negative reversal potential (the equilibrium potential for Cl^- under these conditions being −66 mV). The channel's selectivity for K^+ over Na^+ was demonstrated in experiments in which voltage ramps were applied to a patch in the presence of standard saline (external face) and K^+–aspartate solution (internal face). As illustrated in Fig. 10*D*, current through the channel was outward at even the most negative potential imposed, −73 mV. For these ionic conditions, the constant-field equation (Hodgkin & Katz, 1949) indicates a permeability ratio, P_{Na}/P_K, of less than 0·05. The channel's high selectivity for K^+ over Na^+ is consistent with that measured for the Ca^{2+}-activated K^+ conductance in whole cells; under similar ionic conditions the whole-cell tail current reverses at −82 mV (Lewis & Hudspeth, 1983*b*). The magnitude of the single-channel current at −30 mV (4·2 pA; Fig. 10*D*), is somewhat larger than estimates based on ensemble-variance analysis of whole-cell $I_{K(Ca)}$ (1·1–2·6 pA) at the same potential. In the period shortly after the establishment

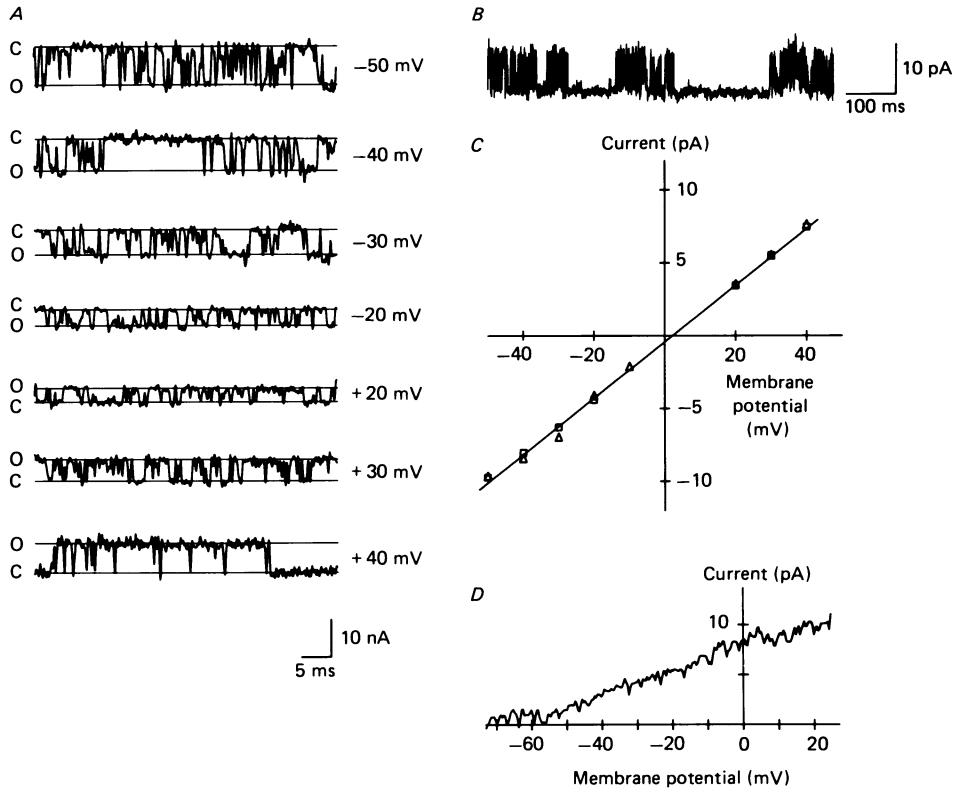

Fig. 10. Conductance and selectivity of the Ca^{2+}-activated K^+ channel. *A*, current through a single Ca^{2+}-activated K^+ channel in an inside-out patch, recorded in symmetrical [K^+]. The holding potential is given to the right of each trace; the closed- and open-channel current levels, measured from peaks in current-amplitude histograms, are indicated by lines marked 'C' and 'O' on the left. Cell 2; internal (bath) solution, KCl + 100 μM-Ca^{2+}; external (pipette) solution, KCl saline. *B*, Ca^{2+}-activated K^+ channel current displayed on a slower time scale to show long closing events. Same patch and ionic conditions as in *A*; holding potential, −40 mV. *C*, current–voltage relation of the Ca^{2+}-activated K^+ channel. Same patch and conditions as in *A*. current values were determined from amplitude histograms. A line fitted to the data points by linear regression indicates a slope conductance of 195 pS and a reversal potential of 1·3 mV. The conductance and reversal potential were unaffected by varying internal Ca^{2+} concentration from 10 μM(△) to 100 μM(□). *D*, averaged current–voltage relation of a single Ca^{2+}-activated K^+ channel, obtained from ramp-clamp data under ionic conditions similar to those used in whole-cell recording (internal solution, K^+–aspartate + 100 μM-Ca^{2+}; external solution, standard saline). A linear-regression fit at potentials between −40 and 0 mV indicates a slope conductance of 124 pS. The current did not reverse in sign for voltages as negative as −73 mV, demonstrating a high degree of selectivity for K^+ over Na^+. Data were filtered at 1 kHz and sampled at 200 μs intervals. Cell 15.

of the whole-cell recording configuration when ensemble-variance records were obtained, however, the membrane potential may have been biased by −10 to −15 mV relative to the command voltage by a Donnan potential between the pipette and the cell's interior. This error would not apply to excised-patch recordings because of rapid equilibration of intracellular ions with the bath solution (Fernandez

et al. 1984). Thus, to compare single-channel amplitudes with estimates made from ensemble-variance analysis, it may be more appropriate to measure the single-channel current at −40 to −45 mV; at these potentials the data in Fig. 10*D* indicate values of 2·1–2·8 pA, which fall within the range estimated from ensemble-variance experiments.

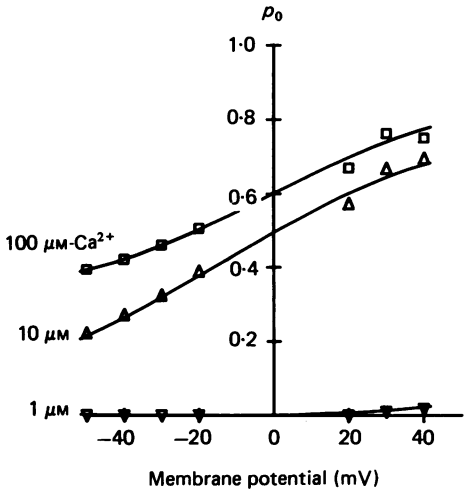

Fig. 11. Dual dependence of Ca^{2+}-activated K^+-channel activity on $[Ca^{2+}]_i$ and membrane potential. Current through a single Ca^{2+}-activated K^+ channel in an inside-out patch was recorded at holding potentials of −50 to +40 mV in the presence of 1, 10, or 100 μM-Ca^{2+} bathing the intracellular face. Segments of activity (3·3 s) were scanned for opening and closing transitions and the open-state probability (p_o) was calculated as the total fraction of time spent in the open state. Increasing $[Ca^{2+}]_i$ and membrane depolarization promote channel activity. Cell 2; internal solution, KCl + 1 μM-Ca^{2+}(▽), KCl + 10 μM-Ca^{2+}(△) or KCl + 100 μM-Ca^{2+}(□); external solution, KCl saline.

The dual Ca^{2+} and voltage dependence of the channel's activity is demonstrated in Fig. 11. For holding potentials of −50 to 40 mV and for 1, 10 and 100 μM-internal Ca^{2+}, we examined the recorded activity for channel-opening and -closing transitions. The open-state probability, p_o, was estimated from the fraction of time a given channel spent in the open state. As shown here, an increase in $[Ca^{2+}]_i$ or a depolarization can activate the channel. It is interesting to note that relatively high concentrations of internal Ca^{2+} are required to activate the channel at physiologically relevant potentials (i.e. between −60 and −20 mV). This rather low Ca^{2+} sensitivity was observed in nine other patches; assuming that channels in excised patches behave as they do in the intact cell, these results imply that $[Ca^{2+}]_i$ must rise to high levels (> 100 μM) to account for the open-state probability near 0·8 measured at −30 mV in intact cells. The hair cell's K^+ channel shows approximately the same sensitivity to $[Ca^{2+}]_i$ as the 'maxi' K^+ channel from rat muscle, but is less voltage dependent (Barrett, Magleby & Pallotta, 1982; Moczydlowski & Latorre, 1983).

In summary, the prevalence, K^+ selectivity, unitary conductance and Ca^{2+}-dependent activation of this channel strongly suggest that it underlies the hair cell's Ca^{2+}-activated K^+ conductance. For these reasons, we shall hereafter refer to this channel as the Ca^{2+}-activated K^+ channel.

Kinetic states of the Ca^{2+}-activated K^+ channel. The minimum number of kinetic states of the Ca^{2+}-activated K^+ channel was deduced from steady-state distributions of open- and closed-channel lifetimes. Quantitative estimation of rate constants for transitions among the states was unfortunately precluded by slow changes in channels' behaviour and by differences among the four patches that were examined in detail. Conclusions regarding the number of states were consistent, however, and support the following five-state gating scheme, a modification of models proposed by Magleby & Pallotta (1983) and Moczydlowski & Latorre (1983):

$$C_0 \underset{k_{-1}}{\overset{k_1[Ca^{2+}]_i}{\rightleftharpoons}} C_1 \underset{k_{-2}}{\overset{k_2[Ca^{2+}]_i}{\rightleftharpoons}} C_2 \underset{\alpha_C}{\overset{\beta_C}{\rightleftharpoons}} O_2 \underset{k_{-3}}{\overset{k_3[Ca^{2+}]_i}{\rightleftharpoons}} O_3. \qquad (7)$$

C and O are closed and open states respectively and the subscripts denote the number of Ca^{2+} ions bound. k_1, k_2, and k_3 are rate constants for Ca^{2+} binding, and k_{-1}, k_{-2}, and k_{-3} are those for Ca^{2+} release. α_C and β_C are respectively the channel's closing and opening rate constants. More complete studies of Ca^{2+}-activated K^+ channels in other cells have indicated that their gating mechanism is considerably more complex than is indicated here (Magleby & Pallotta, 1983); we present this scheme only as the simplest one that incorporates three closed and two open states. The data supporting the number of states in this scheme are described below.

Under conditions of constant membrane potential and $[Ca^{2+}]_i$, open-lifetime distributions were well described by a single-exponential function with a time constant that increased with $[Ca^{2+}]_i$. For the patch of Fig. 12*A*, raising $[Ca^{2+}]_i$ from 10 to 100 μM at a membrane potential of 30 mV increased the mean open time from 0·76 to 1·03 ms. The simplest interpretation of this result is that there are two open states of the channel in rapid equilibrium with each other (Moczydlowski & Latorre, 1983). If binding and unbinding of Ca^{2+} from the open states is much faster than the closing transition, this scheme predicts a single-exponential open-time distribution that is lengthened by increasing $[Ca^{2+}]_i$.

The duration of channel opening was also voltage dependent in the presence of constant $[Ca^{2+}]_i$; depolarization prolonged opening. For the patch of Fig. 12 exposed to 10 μM-Ca_i^{2+}, changing the potential from -50 to 40 mV increased the mean open lifetime from 0·28 to 0·88 ms. In terms of eqn (7), this result indicates that at least some of the rate constants α_C, k_3, and k_{-3} are voltage dependent.

Because the closed lifetimes of the Ca^{2+}-activated K^+ channel were fitted by the sum of two exponential distributions (Fig. 12*B*), there must be at least two closed states. The presence of an additional, long-lived closed state was suggested by closures lasting 100–500 ms that occurred even at moderate levels of activation (see Fig. 10*B*). These events were too frequent to be a likely part of the 1–2 ms closed-time distribution, but were too infrequent to produce an obvious third exponential component in the closed-time histogram given the 3·3 s sampling period at each potential. Closed-channel lifetimes decrease with increasing $[Ca^{2+}]_i$. In Fig. 12*B*, raising $[Ca^{2+}]_i$ from 10 to 100 μM at a membrane potential of -40 mV reduced the average closed duration from 0·96 to 0·59 ms. The Ca^{2+} dependence of closed lifetime indicates that Ca^{2+} binds to one or more closed states to bias the channel towards opening. By analogy to the model of Magleby & Pallotta (1983), we have arbitrarily assumed in eqn (7) that two Ca^{2+} ions bind before the channel can open.

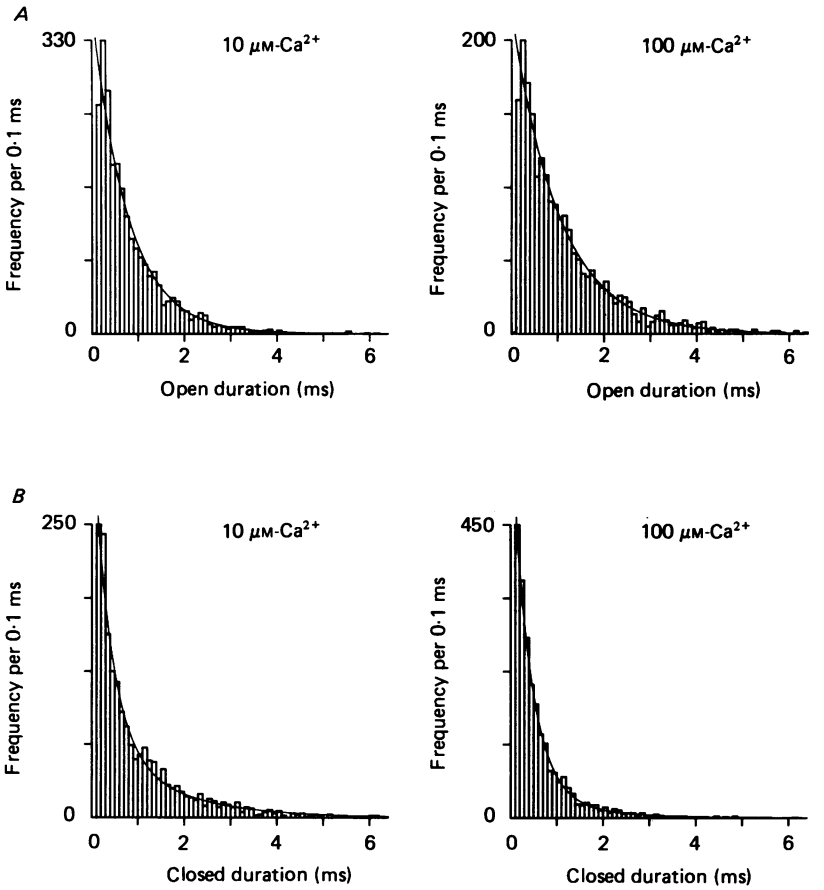

Fig. 12. Dependence on Ca^{2+} of the open and closed lifetimes of the Ca^{2+}-activated K^+ channel. Same patch and experimental conditions as in Fig. 10. *A*, open-lifetime distribution at +30 mV in the presence of 10 μM- (left) or 100 μM-internal Ca^{2+} (right). These distributions were best fitted by single-exponential conditional-probability-density functions (eqn (4)) with $\tau = 0{\cdot}76$ ms (10 μM-Ca_i^{2+}) or $\tau = 1{\cdot}03$ ms (100 μM-Ca_i^{2+}). The probability-density functions have been scaled by the number of observed events and are superimposed on each histogram. *B*, closed-lifetime distribution at −40 mV in the presence of 10 μM- (left) or 100 μM-internal Ca^{2+} (right). Closed-time distributions were best described by double-exponential functions (eqn (4); $a_1 = 0{\cdot}51$, $\tau_1 = 0{\cdot}39$ ms, $a_2 = 0{\cdot}49$, $\tau_2 = 1{\cdot}56$ ms for 10 μM-Ca^{2+}; $a_1 = 0{\cdot}82$, $\tau_1 = 0{\cdot}40$ ms, $a_2 = 0{\cdot}18$, $\tau_2 = 1{\cdot}45$ ms for 100 μM-Ca^{2+}). Scaled forms of these curves are superimposed on the histograms. Elevation of $[Ca^{2+}]_i$ effects a decrease in the average closed lifetime from 0·96 ms (10 μM-Ca^{2+}) to 0·58 ms (100 μM-Ca^{2+}).

Closed lifetime was also voltage dependent, decreasing with membrane depolarization. For the patch of Fig. 12 exposed to 10 μM-Ca_i^{2+}, changing the potential from −50 to 40 mV reduced the average closed duration from 1·2 to 0·3 ms. This result suggests that at least some of the rate constants k_1, k_{-1}, k_2, k_{-2}, and β_C in eqn (7) are voltage dependent.

Kinetic behaviour of Ca^{2+}-activated K^+ channels opened by voltage pulses. To obtain

more information about their voltage dependence, we activated K^+ channels by depolarization in the presence of constant $[Ca^{2+}]_i$. Individual responses of a single K^+ channel are shown in Fig. 13*A*; at the holding potential of −93 mV the channel was almost always closed, but depolarization to +87 mV opened it, producing a rapidly fluctuating outward current of 12 pA amplitude. The overall time course of opening and closing was obtained by averaging the responses to 124 consecutive potential pulses (Fig. 13*B*).

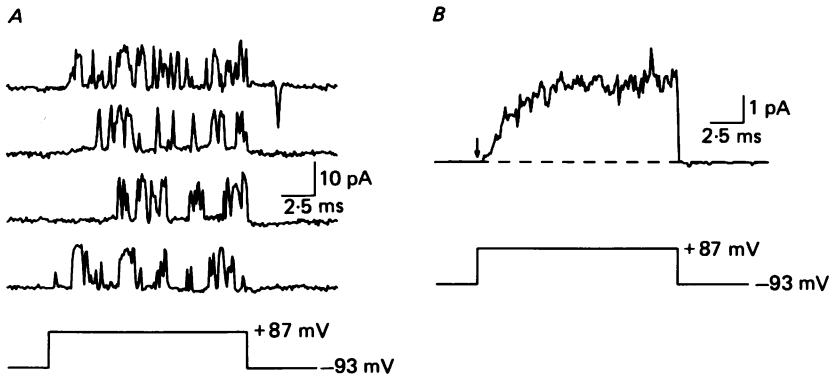

Fig. 13. Voltage-dependent activation of the Ca^{2+}-activated K^+ channel. *A*, four responses of a single channel in an inside-out patch to a voltage-clamp pulse from −93 to +87 mV. At the holding potential of −93 mV, the channel was closed over 99% of the time, but depolarization to +87 mV opened the channel, resulting in a rapidly fluctuating outward current. Rare openings at −93 mV produced inward current (top trace). *B*, average of 124 consecutive responses to the stimulus in *A*. On average, the channel opened with a sigmoidal time course following an apparent lag of 0·5 ms, a result consistent with the existence of multiple closed states, and closed rapidly upon repolarization. Cell 136; internal solution, K^+–aspartate + 8 μM-Ca^{2+}; external solution, KCl saline.

The time courses for activation and deactivation of the averaged single-channel current have important implications for kinetic models of the channel and for explaining the kinetic features of $I_{K(Ca)}$ in whole-cell recordings. Like the macroscopic $I_{K(Ca)}$, the averaged single-channel current increases with a sigmoidal time course, producing the first measurable outward current about 0·5 ms after the start of the voltage pulse. Because $[Ca^{2+}]_i$ in this experiment was constant, the latency of activation did not result from the diffusion of Ca^{2+} ions from Ca^{2+} channels to K^+ channels, a process that may be of importance in whole-cell experiments. The latency must have resulted instead from transitions through multiple closed states of the Ca^{2+}-activated K^+ channel on its way to opening (eqn (7)). Channel closing was rapid upon repolarization to −93 mV; the average current returned to baseline within one sampling interval, or 100 μs, with very few reopenings (Fig. 13*B*). In a similar experiment on another patch, repolarization to −53 mV caused the average current to decline exponentially with a time constant of 0·4 ms. Slowing of the deactivation rate with depolarization would be expected from the voltage dependence of open lifetimes measured under steady-state conditions, as described above.

Modelling the Ca^{2+}-activated K^+ current

In this section we describe a model that links the intracellular free Ca^{2+} concentration, $[Ca^{2+}]_i$, controlled by Ca^{2+}-channel activity and Ca^{2+}-regulation processes, to the activation of Ca^{2+}-activated K^+ channels. The model, represented diagramatically in Fig. 14, presents the activation of $I_{K(Ca)}$ following a step depolarization of the cell membrane as a sequence of three interacting processes.

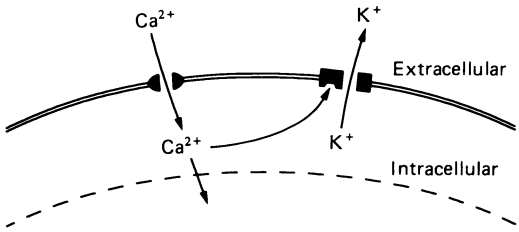

Fig. 14. A model for the activation of Ca^{2+} and Ca^{2+}-activated K^+ currents in the hair cell. The double line represents the plasma membrane, with intra- and extracellular spaces as shown. Membrane depolarization initiates a sequence of three interactive processes. (1) voltage-dependent Ca^{2+} channels open as described by a third-order kinetic scheme. (2) calcium enters the cell and accumulates in a space subjacent to the membrane, bounded schematically by the dotted line. (3) Calcium in this space acts to open Ca^{2+}-activated K^+channels, as described by a five-state kinetic scheme presented in the text. Calcium leaves this space at a rate proportional to its concentration. This simplified first-order form of Ca^{2+} regulation is intended to approximate the combined effects of diffusion, sequestration and active transport.

First, depolarization opens voltage-dependent Ca^{2+} channels in accordance with the kinetic scheme outlined in eqns (5) and (6). Next, Ca^{2+} entering the cell accumulates in a space subjacent to the membrane and acts to open Ca^{2+}-activated K^+ channels as described by eqn (7). Finally, Ca^{2+} is removed from the submembrane compartment at a rate proportional to its concentration. The complete set of equations that the model comprises is presented in the Appendix.

The rationale we used to constrain the values of parameters in the model is outlined below and detailed in the Appendix. First, the parameter values related to Ca^{2+}-channel gating were determined directly from measurements of I_{Ca} (Fig. 6). Values for the remaining parameters, pertaining to Ca^{2+} regulation and the gating of Ca^{2+}-activated K^+ channels, were then adjusted to provide the best fits to Ca^{2+}-activated K^+ currents recorded in the same cell from which the Ca^{2+} currents were recorded (Figs 6 and 7). Rough limits imposed on the values of Ca^{2+}-regulation parameters by whole-cell and single-channel data are noted in the Appendix.

The best fits of the model to a series of whole-cell Ca^{2+}-activated K^+ currents are shown in Fig. 15. Aside from some minor discrepancies, it appears that the model provides an accurate empirical description of the time course and magnitude of $I_{K(Ca)}$ elicited at potentials between -55 and -30 mV. The parameter values used to generate these predictions are listed in Table 2.

Testing the model: predictions of the Ca^{2+} and voltage dependence of $I_{K(Ca)}$. Because of the model's large number of free parameters, we were concerned that the specific

values we chose to fit a particular example of the Ca^{2+}-activated K^+ current might not accurately reflect the current's true activation mechanism. The model might therefore fail to predict other responses correctly, for example those under current-clamp conditions. Regardless of the assumptions made about the activation of $I_{K(Ca)}$, any sufficiently complex model can in principle predict the correct waveform of

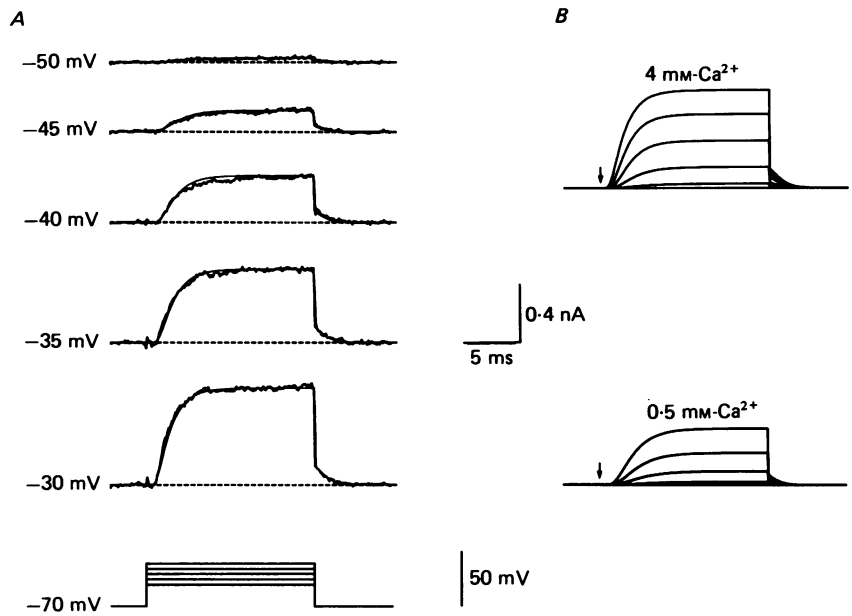

Fig. 15. Model predictions of whole-cell Ca^{2+}-activated K^+ current. *A*, after the Ca^{2+} currents of Fig. 6 were fitted with a third-order kinetic scheme, values for the remaining model parameters were selected to generate the best fits to $I_{K(Ca)}$ recorded in the same cell. Values are listed in Table 2. The model predictions (smooth traces) are shown superimposed on the Ca^{2+}-activated K^+ currents from Fig. 7*A*. The values of the voltage-command pulses represented at the bottom are listed in millivolts to the left of each trace. *B*, model simulations of the effect on $I_{K(Ca)}$ of reducing extracellular $[Ca^{2+}]$. The model's predictions of $I_{K(Ca)}$ elicited at the same potentials as in Fig. 8*B* are shown for 4 mM- (top) and 0·5 mM-Ca_o^{2+} (bottom). Responses in 4 mM-Ca^{2+} were generated using the parameter values in Table 2; for the low-Ca^{2+} condition $\bar{g}_{Ca}$ in the model was reduced by 75%, based on the results in Fig. 8*A*.

$I_{K(Ca)}$ at each potential. Provided with a sufficient number of channel states, a model based upon a purely voltage-dependent K^+ conductance could undoubtedly fit the Ca^{2+}-activated K^+ currents observed in whole-cell recordings. Because it could not account for the changes in $I_{K(Ca)}$ brought about by altering Ca^{2+} influx or by modifying the cell's Ca^{2+}-regulation mechanisms, however, such a model would have a somewhat restricted predictive ability.

To assess the accuracy of our description of the relative sensitivity of $g_{K(Ca)}$ to Ca^{2+} and membrane potential, we tested the model's ability to simulate the effects of reduced $[Ca^{2+}]_o$ on the activation of $I_{K(Ca)}$. For this purpose, we reduced the maximal Ca^{2+}-conductance term in the model, $\bar{g}_{Ca}$, by 75%, an amount consistent with the experimental effect on I_{Ca} of lowering $[Ca^{2+}]_o$ from 4 to 0·5 mM (Fig. 8*A*).

The model's simulations of $I_{K(Ca)}$ under this and the control conditions are shown in Fig. 15*B*. In qualitative agreement with the experimental results (Fig. 8*B*), the model predicts a decrease in both the magnitude and speed of $I_{K(Ca)}$ activation when external [Ca^{2+}] is reduced. On the basis of this test, the model thus appears to provide a reasonable description of the Ca^{2+}- and voltage-dependent activation of the hair cell's Ca^{2+}-activated K^+ conductance.

TABLE 2. Values of model parameters

Parameter	Value	Parameter	Value
$\bar{g}_{Ca}$	4·14 nS	$\bar{g}_{K(Ca)}$	16·8 nS
E_{Ca}	100 mV	E_K	−80 mV
α_0	22800 s^{-1}	$K_1(0)$	6 μM
V_0	70 mV	D_1	0·2
V_A	8·01 mV	k_{-1}	300 s^{-1}
K_A	510 s^{-1}	$K_2(0)$	45 μM
β_0	0·97 s^{-1}	D_2	0
V_B	6·17 mV	k_{-2}	5000 s^{-1}
K_B	940 s^{-1}	$K_3(0)$	20 μM
U	0·02	D_3	0·2
ξ	$3·4 \times 10^{-5}$	k_{-3}	1500 s^{-1}
C_{vol}	1·25 pl	$\alpha_C(0)$	450 s^{-1}
K_S	2800 s^{-1}	V_a	33 mV
		β_C	1000 s^{-1}

DISCUSSION

Whole-cell recording from solitary hair cells

The method we employed to dissociate hair cells from the sacculus, a combination of proteolytic treatment and mechanical scraping, is likely to affect the integrity of membrane ionic conductances in these cells. Such effects would explain the variable magnitudes of Ca^{2+} and leakage conductances we observed in cells isolated from different sacculi and the relatively low incidence of solitary hair cells that displayed electrical resonance. Because both the Ca^{2+} current and the Ca^{2+}-activated K^+ current could be recorded in the same cell, however, cellular damage did not pose a serious problem in our attempts to relate the two currents.

The whole-cell recording configuration itself also modifies the electrical properties of the cell, in particular causing a slow, irreversible decline in the magnitude of the Ca^{2+} conductance. This decline in g_{Ca} may be responsible for decreases in $g_{K(Ca)}$ and in the best frequency and sharpness of the cell's electrical resonance that we observed over a similar time period. Run-down of I_{Ca} has been reported for a number of internally dialysed preparations (Byerly & Hagiwara, 1982; Fenwick, Marty & Neher, 1982). Although ATP in the intracellular solution can prevent the decline of I_{Ca} in molluscan neurones (Byerly & Yazejian, 1986), in our recordings from hair cells the addition to the internal solution of 2·5 mM-ATP, 0·5 mM-GTP and 2 mM-Mg^{2+} had no noticeable effect. We therefore had to collect voltage- and current-clamp data during the first few minutes of whole-cell recording, while g_{Ca} was constant. This temporal restriction had two consequences: it prevented the collection of extensive

voltage- and current-clamp data from the same cell and did not allow enough time for the complete dissipation of a putative Donnan potential between the pipette and the cell's interior. Because the Donnan potential offsets the membrane potential equally in voltage- and current-clamp recordings, it does not compromise comparisons between the two types of data. It should be noted, however, that the whole-cell potentials reported in this and the companion paper (Hudspeth & Lewis, 1988) may be shifted by +10 to +15 mV relative to recordings made with conventional, high-resistance microelectrodes.

Ionic conductances: comparisons and functional implications

A-conductance. The time courses of activation and inactivation of the hair cell's A-conductance are similar to those reported for molluscan neurones (Connor & Stevens, 1971; Neher, 1971). Two important differences, however, are that the voltage dependence of I_A activation and inactivation in the hair cell do not appreciably overlap (Figs 3*B* and 4*B*) and that the hair cell's A-conductance is completely inactivated at the resting potential under steady-state conditions (Fig. 4*B*). As a result, I_A is unlikely to be active during potential oscillations elicited by depolarization from the resting potential (Fig. 1*A*). In molluscan neurones and crab axons, I_A is believed to help regulate the frequency of repetitive firing (Connor, 1978). The voltage dependence of I_A in the hair cell, and the fact that hair cells do not normally produce action potentials, rule out such a function in this cell. Although its role in the hair cell is unknown, I_A may become activated by rapid depolarization after a relatively long hyperpolarization, such as might result from mechanical stimulation following a burst of activity of the hair cell's efferent nerve supply (Art, Fettiplace & Fuchs, 1984).

Ca^{2+} conductance. The hair cell's Ca^{2+} conductance is slightly activated at the resting potential and does not inactivate during moderate depolarizations (Lewis & Hudspeth, 1983*b*; Ohmori, 1984; Art & Fettiplace, 1987). Both of these characteristics are consistent with a role in the release of transmitter from hair cells, which is known to be Ca^{2+} dependent (Furukawa & Matsuura, 1978) and to occur tonically at the resting potential (Sand, Ozawa & Hagiwara, 1975; Sewell, 1984). Similar properties have been reported for the Ca^{2+} conductance in rod photoreceptors (Corey, Dubinsky & Schwartz, 1984), cells that also release transmitter continuously in the absence of a sensory stimulus. The steady Ca^{2+} current at the resting potential may contribute to the spontaneous activity observed in auditory-afferent nerve fibres and allow the postsynaptic fibres to encode responses to both depolarizations and hyperpolarizations of hair cells (Crawford & Fettiplace, 1981), resulting respectively from positive and negative deflections of hair bundles.

The activation of the Ca^{2+} conductance in saccular hair cells is quite rapid, substantially faster than that reported for g_{Ca} in several other cell types (chromaffin cells, Fenwick *et al.* 1982; clonal pituitary cells, Hagiwara & Ohmori, 1982; rod photoreceptors, Corey *et al.* 1984). Ca^{2+} currents with similarly rapid time courses have been reported in hair cells from the chick's vestibular apparatus (Ohmori, 1984) and from the turtle's basilar papilla (Art & Fettiplace, 1987). The high speed of I_{Ca} in the hair cell may be required for the cell's ability to convey information about the phase of sound at frequencies up to 9 kHz (Sullivan & Konishi, 1984). In contrast,

the requirement for speed is less critical for cells such as adrenal chromaffin and pituitary cells, whose function is the slow, sustained release of hormones or transmitters, and for photoreceptors, whose electrical response has a relatively slow time course.

Ca^{2+}-activated K^+ conductance. The Ca^{2+}-activated K^+ conductance is the largest ionic conductance in the hair cell, dominating the steady-state current–voltage relation at potentials positive to the resting potential (Corey & Hudspeth, 1979; Ohmori, 1984; Ashmore & Meech, 1986; Art & Fettiplace, 1987). The most conspicuous features of the whole-cell Ca^{2+}-activated K^+ current are its extremely rapid activation and deactivation and the steep dependence of its activation on membrane potential in the range just positive to the resting potential. These features enable $I_{K(Ca)}$ to participate in electrical resonance at frequencies of 90–250 Hz, a function considered in detail in the companion paper (Hudspeth & Lewis, 1988). In addition, as discussed below, the kinetic behaviour and Ca^{2+} dependence of $I_{K(Ca)}$ have possible implications for the nature of intracellular Ca^{2+} regulation.

The $I_{K(Ca)}$ in the hair cell (Lewis & Hudspeth, 1983*b*; Art & Fettiplace, 1987) is activated 10–1000 times faster than its counterpart in a number of invertebrate and vertebrate cell types (molluscan neurones: Meech & Standen, 1975; Barish & Thompson, 1983; neuroblastoma: Moolenaar & Spector, 1979; pituitary tumour: Dubinsky & Oxford, 1984), but with a time course comparable to that of I_C described in bull-frog sympathetic neurones (Adams, Constanti, Brown & Clark, 1982; Brown, Constanti & Adams, 1983). Studies using Ca^{2+}-sensitive dyes have shown that the time course of $I_{K(Ca)}$ activation and deactivation in molluscan neurones parallels the time course of change in $[Ca^{2+}]_i$, a result that suggests that the rate of intracellular Ca^{2+} regulation determines the kinetic properties of the Ca^{2+}-activated K^+ current (Ahmed & Connor, 1979; Gorman & Thomas, 1980). The question then arises whether the much faster kinetic behaviour of $I_{K(Ca)}$ in the hair cell is similarly determined by the regulation of the intracellular Ca^{2+} concentration. A definitive answer to this question awaits direct measurements of $[Ca^{2+}]_i$ and of the intrinsic voltage dependence of the cell's Ca^{2+}-activated K^+ channels. Indirect evidence suggests, however, that Ca^{2+} regulation in the hair cell is rapid. For example, in whole-cell recordings, $I_{K(Ca)}$ elicited by submaximally activating potential pulses reaches a steady-state value within 5–10 ms (Fig. 7*A*). If the K^+ channel's Ca^{2+} sensor is not saturated during these stimuli, $[Ca^{2+}]_i$ must attain a steady level within this same period; this implies a rapid rate of Ca^{2+} redistribution. One alternative to such a proposal is that Ca^{2+} regulation is slow, but that the K^+ channel is quickly saturated with Ca^{2+}, so that the time course of $I_{K(Ca)}$ mainly reflects the voltage-dependent properties of the channel. This notion is compatible with observations of the Ca^{2+}-activated K^+ current, I_C, in sympathetic neurones (Adams *et al.* 1982; Brown *et al.* 1983), for which deactivation is much faster than the time course of intracellular Ca^{2+} transients (Smith, MacDermott & Weight, 1983). Such a scheme is not consistent with the effects of $[Ca^{2+}]_o$ on $I_{K(Ca)}$ magnitude in the hair cell, however, which suggests that the channel's Ca^{2+} sensor is not saturated during small depolarizations (see Fig. 8). Rapid regulation of $[Ca^{2+}]_i$ can also be inferred from phase locking of responses of the turtle's auditory nerve to tone bursts (Crawford & Fettiplace, 1980). If the postsynaptic response is a constant function of presynaptic

$[Ca^{2+}]_i$, any accumulation of Ca^{2+} in the hair cell during successive cycles of a stimulus tone would progressively widen the peaks of the postsynaptic spike histogram, and phase locking would be expected to decline. The observed constancy of phase-locking at stimulus frequencies of at least 265 Hz therefore indicates that $[Ca^{2+}]_i$ in the hair cell returns to essentially its baseline level between successive stimulus cycles. The inferred rapidity of Ca^{2+} fluctuations in this case contrasts markedly with the much slower Ca^{2+} regulation in molluscan bursting-pacemaker neurones, in which Ca^{2+} accumulates steadily during a 0·5 Hz train of brief depolarizations (Gorman & Thomas, 1980). Because $I_{K(Ca)}$ is slow in GH pituitary-tumour cells of comparable size (Dubinsky & Oxford, 1984), the relatively small size of the hair cell apparently does not explain its capacity for rapid Ca^{2+} regulation. Instead, the rate at which intracellular $[Ca^{2+}]$ is controlled is presumably related to a cell's functions; like the speed of the hair cell's Ca^{2+} conductance, the proposed rapidity of its Ca^{2+} regulation mechanisms may be a prerequisite for transmission of high-frequency stimulus information.

The high open-state probability of Ca^{2+}-activated K^+ channels deduced from ensemble-variance measurements, combined with the channels' sensitivity to Ca^{2+} in excised patches, suggests that intracellular Ca^{2+} may reach levels exceeding 100 μM at its site of action on K^+ channels. Such a high concentration is theoretically possible if the incoming Ca^{2+} is concentrated in a restricted space, for example by buffered diffusion (see Appendix). Intracellular Ca^{2+} accumulation would also explain our occasional detection of $I_{K(Ca)}$ in cells in which I_{Ca} was unmeasurably small. Because $I_{K(Ca)}$ was eliminated in such cells by divalent cations that block Ca^{2+} channels, such as Ni^{2+} and Co^{2+}, it appears that Ca^{2+} can in certain circumstances enter the cell too slowly to carry an appreciable current, yet may accumulate next to the membrane to concentrations sufficient to activate $I_{K(Ca)}$. Substantial Ca^{2+} accumulation subjacent to the plasma membrane is also suggested by the inability of Ca^{2+}-free internal solutions containing up to 10 mM-EGTA to prevent activation of $I_{K(Ca)}$ in whole cells, a result also obtained in adrenal chromaffin cells (Marty & Neher, 1985). One alternative to a scheme involving restricted Ca^{2+} diffusion is that a small influx of Ca^{2+} might cause the release of a larger amount of Ca^{2+} from intracellular storage sites.

An overestimate of the open-state probability of Ca^{2+}-activated K^+ channels from fluctuation analysis, or an underestimate of their Ca^{2+} sensitivity, would alleviate the need in our model for such an extreme accumulation of intracellular Ca^{2+}. In the fluctuation analysis, inaccuracies could arise from the method used to isolate $I_{K(Ca)}$, in which a waveform describing the average time course of I_{Ca} was subtracted from the total current (see Methods). Several arguments indicate, however, that this current-isolation method is unlikely to introduce significant errors. First, similar results were obtained in experiments in which the actual Ca^{2+} currents, rather than approximations, were employed in the isolation of $I_{K(Ca)}$ (L. Robles W., W. M. Roberts & A. J. Hudspeth, unpublished observations). Moreover, the kinetic behaviour of I_{Ca} is so similar among saccular hair cells (Roberts *et al.* 1986) that the corrected grand-average current should accurately reflect the waveform of $I_{K(Ca)}$. Finally, the current variance due to Ca^{2+}-channel gating, as calculated from eqns (1) and (2), is only a small fraction of the total variance. Using values of $i = -0{\cdot}12$ pA,

as estimated in chromaffin cells for recording conditions similar to ours (Fenwick *et al.* 1982), and $p = 0{\cdot}42 \pm 0{\cdot}06$ (S.D., $n = 4$ cells) and $I = -236 \pm 218$ pA (S.D., $n = 26$ cells) from hair cell measurements, the calculated variance of I_{Ca} at -30 mV is at most 35 pA^2, or less than 4% of the total observed variance. Consistent with this estimate, the observed variance did not increase significantly between the start of a voltage-clamp pulse and the time at which $I_{K(Ca)}$ started to appear, a period during which I_{Ca} nearly reached its maximum value.

Alternatively, damage to the Ca^{2+}-sensing mechanism of the Ca^{2+}-activated K^+ channels by our excised-patch recording procedures could lead to an underestimate of their Ca^{2+} sensitivity. Although we cannot exclude this possibility at present, all of the Ca^{2+}-activated K^+ channels that were studied in excised patches showed roughly equal dependencies on internal $[Ca^{2+}]$. It is worth noting that while the Ca^{2+} sensitivity we have observed is lower than those of Ca^{2+}-activated K^+ channels in several preparations, they are similar to that reported for the 'maxi' K^+ channel in rat muscle (Barret *et al.* 1982; Moczydlowski & Latorre, 1983). A more rigorous assessment of the condition of the channel in excised patches awaits a comparison of channel behaviour in cell-attached and excised-patch configurations.

Modelling the Ca^{2+}-activated K^+ current

In order to model the Ca^{2+}-activated K^+ current, we adopted a linear, five-state gating scheme for the Ca^{2+}-activated K^+ channel. The transition rate constants in the scheme were chosen to fit whole-cell $I_{K(Ca)}$ data, and, probably as a consequence, the scheme in its final form is not wholly consistent with single-channel behaviour. One discrepancy is that the values chosen for the rates of Ca^{2+} binding and unbinding from the open states are too low to predict a single-exponential distribution of open-channel lifetimes at negative potentials, although the predicted open times are in the correct range. This inconsistency might have been avoided by making one or more of the reverse rate constants (k_{-1}, k_{-2} and k_{-3}) voltage dependent or by introducing a term describing Ca^{2+} diffusion from its site of entry, the Ca^{2+} channel, to its target, the K^+ channel. These alterations were not made because of the increased number of free parameters such changes would introduce into the model. It is worth noting that while Ca^{2+} diffusion time is likely to contribute to the delay between activation of I_{Ca} and $I_{K(Ca)}$, a significant delay in opening can also result from time-dependent transitions of the K^+ channel through multiple closed states (Fig. 13*B*).

Other schemes describing the gating of Ca^{2+}-activated K^+ channels could be adjusted to fit whole-cell $I_{K(Ca)}$ recorded at any single potential but not over the entire range of -55 to -30 mV. These include the gating scheme of Magleby & Pallotta (1983), which does not incorporate voltage dependence of transition rates, and the four-state scheme of Moczydlowski & Latorre (1983), as well as a simple model in which the magnitude of $g_{K(Ca)}$ is assumed to be at all times at equilibrium with regard to $[Ca^{2+}]_i$ (Lewis, 1984*b*). Interestingly, the last model has been used successfully to simulate the slow modulatory activities of $I_{K(Ca)}$ in a variety of cells (e.g. Smith, 1978), as well as electrical resonance in hair cells (Ashmore & Attwell, 1985). The inability of such a model to describe $I_{K(Ca)}$ in the hair cell adequately may arise because the hair cell regulates its intracellular calcium on a rapid time scale, one comparable to the transition rates of the Ca^{2+}-activated K^+ channel. We did not

attempt to fit purely voltage-dependent models to the $I_{K(Ca)}$ data. Although such schemes can approximate the current's time course of activation reasonably well at a single potential (Art & Fettiplace, 1987), they conceal the contribution of intracellular-Ca^{2+} regulation to the time course of $I_{K(Ca)}$ and consequently to its functions in the cell.

The model we have presented is certainly not the only one capable of describing the characteristics of $I_{K(Ca)}$ in the hair cell, even though it is probably one of the simplest. The model contains a large number of free parameters relating to the gating of Ca^{2+}-activated K^+ channels, values for which can be accurately determined only through a more complete study of these channels. We have also observed that the degree of coupling between Ca^{2+} and Ca^{2+}-activated K^+ currents, presumably a function of the characteristics of intracellular Ca^{2+} regulation and the Ca^{2+} sensitivity of K^+ channels, varies among hair cells. The values of many of the model's parameters must therefore be adjusted in order to fit the data from other cells. Nevertheless, in view of the large number of free parameters, it is reassuring that the model can correctly predict the observed changes in $I_{K(Ca)}$ brought about by decreasing $[Ca^{2+}]_0$ (Fig. 15*B*). The description of the Ca^{2+}-activated K^+ conductance, while certainly not unique, is none the less adequate to account for its voltage- and ion-dependent behaviour. The model may therefore be applied to determine the role of Ca^{2+}-activated K^+ channels in shaping the electrical behaviour of the hair cell under current-clamp conditions (Hudspeth & Lewis, 1988).

APPENDIX

Modelling the Ca^{2+}-activated K^+ current

A model presented in the text describes the activation of $I_{K(Ca)}$ in terms of Ca^{2+}-current activation, the resultant accumulation of Ca^{2+} inside the cell, and Ca^{2+}-dependent activation of K^+ channels. The equations and justifications pertaining to these three parts of the model are presented below; certain important equations are repeated from the text. In addition, we describe the nature of constraints on some of the parameter values and the rationale for selecting the final values listed in Table 2.

Ca^{2+} current (I_{Ca}). Voltage-dependent I_{Ca} activation is described by a third-order kinetic scheme (Hodgkin & Huxley, 1952),

$$I_{Ca} = \bar{g}_{Ca}\, m^3 (V_m - E_{Ca}), \tag{5}$$

in which $\bar{g}_{Ca}$ is the limiting value of Ca^{2+} conductance when all Ca^{2+} channels are open, m is the time-dependent value of the activation parameter, V_m is membrane potential, and E_{Ca} is the Ca^{2+} equilibrium potential. The activation parameter, m, varies between zero and unity with time,

$$dm/dt = \beta_m (1-m) - \alpha_m m, \tag{8}$$

in which α_m and β_m are respectively the m gate's closing and opening rate constants. For perturbation by a step change in membrane potential, eqn (8) can be solved for m, yielding

$$m(t) = m_0 + (m_\infty - m_0)[1 - \exp(-t/\tau_m)], \tag{6}$$

in which m_0 is the initial value of m before a potential change and τ_m is the time constant of m's exponential approach to m_∞, its equilibrium value at the new potential.

One may derive α_m and β_m, the opening and closing rate constants for the m gate, from the values of m_∞ and τ_m. If $m_0 = 0$ at holding potentials below -60 mV, τ_m and m_∞ can be expressed in terms of α_m and β_m:

$$\tau_m = 1/(\alpha_m + \beta_m), \tag{9}$$

$$m_\infty = \beta_m/(\alpha_m + \beta_m). \tag{10}$$

α_m and β_m can, in turn, be described as empirical functions of potential:

$$\alpha_m = \alpha_0 \exp[-(V_m + V_0)/V_A] + K_A, \tag{11}$$

$$\beta_m = \beta_0 \exp[(V_m + V_0)/V_B] + K_B, \tag{12}$$

in which α_0, K_A, β_0, and K_B are rate constants and V_0, V_A, and V_B are potentials to be determined experimentally.

Although the activation of the hair cell's voltage-dependent Ca^{2+} current is described well by a second-order (Ohmori, 1984; Art & Fettiplace, 1987) or third-order (Lewis & Hudspeth, 1983*b*) kinetic scheme, the complex time courses of deactivation and single-channel behaviour of Ca^{2+} channels in other preparations (e.g. Fenwick *et al.* 1982) suggest that this formulation does not in general accurately represent the channel's gating mechanism. We accordingly employ this scheme as a convenient empirical description of the Ca^{2+} current's kinetic behaviour rather than as a definitive description of a particular gating mechanism for the channel. Although the current through Ca^{2+} channels is not ohmic at potentials approaching E_{Ca} (Byerly & Hagiwara, 1982; Fenwick *et al.* 1982; Hagiwara & Ohmori, 1982), the simple conductance ($\bar{g}_{Ca}$) and driving force ($V_m - E_{Ca}$) terms in eqn (5) are a good approximation at the potentials considered in this study. Although Ca^{2+} concentration may rise to quite high levels next to the inside surface of the membrane during voltage-clamp pulses, we have also assumed constancy of E_{Ca}. Calcium accumulation is, however, unlikely to affect I_{Ca} significantly; by the constant-field equation (Hodgkin & Katz, 1949), an increase in $[Ca^{2+}]_i$ from 0·1 to 100 μM causes an estimated decrease in I_{Ca} of less than 1% at a potential of -30 mV.

Regulation of intracellular Ca^{2+}. As a convenient description of the processes that control the intracellular Ca^{2+} concentration, we have adopted a relatively simple scheme that was used to describe the inactivation of I_{Ca} caused by Ca^{2+} accumulation in insect skeletal muscle fibres (Standen & Stanfield, 1982). This Ca^{2+}-regulation scheme involves three basic assumptions. First, Ca^{2+} entering the cell binds immediately to an excess of low-affinity intracellular buffers such that a constant fraction, U, of total Ca^{2+} remains free at any given time. Secondly, the binding of Ca^{2+} by relatively immobile buffers slows its diffusion away from the membrane so that Ca^{2+} accumulates next to the membrane in a small fraction, ξ, of the cell's total volume. Thirdly, Ca^{2+} leaves this submembrane compartment at a rate proportional to its free concentration there; the rate constant for this process is K_S. This scheme predicts that, at any given time, the submembrane Ca^{2+} concentration, $[Ca^{2+}]_i$, changes at a rate

$$d[Ca^{2+}]_i/dt = UI_{Ca}/(zFC_{vol}\xi) - K_S[Ca^{2+}]_i, \tag{13}$$

in which z is the valence of Ca^{2+}, F is the Faraday constant, and C_{vol} is the total cell volume, calculated for a cylinder of 8 μm diameter and 25 μm length to be 1·25 pl. Note that a change in U can be compensated by a change in ξ; in fitting the model to hair-cell data we fixed the value of U at 0·02, which corresponds to the estimated proportion of free Ca^{2+} in molluscan neurones (Gorman & Thomas, 1980), and adjusted ξ.

A variety of evidence suggests that this Ca^{2+}-regulation scheme is a reasonable approximation. The effective diffusion coefficient for Ca^{2+} in cytoplasm is lowered by the reversible binding of Ca^{2+} to intracellular buffers (Hodgkin & Keynes, 1957); over short periods of time, this effectively confines incoming Ca^{2+} to a small volume near the membrane. In fact, a spatial gradient of $[Ca^{2+}]_i$ has been observed in molluscan neurones following its influx through Ca^{2+} channels (Smith & Zucker, 1980; Gorman, Levy, Nasi & Tillotson, 1984) and has also been predicted from a model incorporating many of the known features of intracellular Ca^{2+} regulation (Smith, 1978; Smith & Zucker, 1980).

Gating of the Ca^{2+}-activated K^+ channel. The gating of Ca^{2+}-activated K^+ channels in the hair cell is described by a linear, five-state kinetic scheme adapted from earlier models (Magleby & Pallotta, 1983; Moczydlowski & Latorre, 1983). According to this scheme, two intracellular Ca^{2+} ions must bind to the channel to open it, and a third Ca^{2+} ion can then bind to prolong the opening:

$$C_0 \underset{k_{-1}}{\overset{k_1[Ca^{2+}]_i}{\rightleftharpoons}} C_1 \underset{k_{-2}}{\overset{k_2[Ca^{2+}]_i}{\rightleftharpoons}} C_2 \underset{\alpha_C}{\overset{\beta_C}{\rightleftharpoons}} O_2 \underset{k_{-3}}{\overset{k_3[Ca^{2+}]_i}{\rightleftharpoons}} O_3. \tag{7}$$

C_0, C_1 and C_2 represent closed channel states with respectively zero, one, or two Ca^{2+} ions bound, while O_2 and O_3 are open states with respectively two or three Ca^{2+} bound.

Each transition, other than the open–closed transition, is characterized by a Ca^{2+}-dissociation constant, K_j. The voltage dependence of these transitions derives from the assumption that Ca^{2+} binds to a site within the transmembrane electric field (Gorman & Thomas, 1980; Moczydlowski & Latorre, 1983), making the effective dissociation constant a function of membrane potential,

$$K_j(V_m) = K_j(0) \exp[\delta_j z F V_m/(RT)]. \tag{14}$$

$K_j(0)$ is the dissociation constant of the jth binding site at zero transmembrane potential, δ_j is the fraction of the electric field experienced by Ca^{2+} at the jth binding site, and z, F, R, and T have their usual meanings. These dissociation constants are related to the forward and reverse rate constants k_j and k_{-j} by

$$K_j[Ca^{2+}]_i = k_{-j}/k_j. \tag{15}$$

The closing rate constant, α_C, is also expressed as a function of membrane potential,

$$\alpha_C = \alpha_C(0) \exp(-V_m/V_A). \tag{16}$$

$\alpha_C(0)$ is the closing rate constant at 0 mV membrane potential, V_m is membrane potential, and V_A is a potential used to express the voltage dependence of α_C.

If we assume that the mass-action principle applies, the change in occupancy of each state with time is described by a family of differential equations:

$$dC_0/dt = k_{-1}C_1 - k_1[Ca^{2+}]_i C_0, \tag{17}$$

$$dC_1dt = k_1[Ca^{2+}]_i C_0 + k_{-2}C_2 - (k_{-1} + k_2[Ca^{2+}]_i)C_1, \tag{18}$$

$$dC_2/dt = k_2[Ca^{2+}]_i C_1 + \alpha_C O_2 - (k_{-2} + \beta_C)C_2, \tag{19}$$

$$dO_2/dt = \beta_C C_2 + k_{-3}O_3 - (\alpha_C + k_3[Ca^{2+}]_i)O_2, \tag{20}$$

$$dO_3/dt = k_3[Ca^{2+}]_i O_2 - k_{-3}O_3, \tag{21}$$

in which C_i and O_i are the time-dependent probabilities that a channel with i Ca^{2+} ions bound is respectively in the closed or the open state. The summed occupancy of the two open states at any given time gives the probability that the channel is open; therefore

$$g_{K(Ca)} = \bar{g}_{K(Ca)}(O_2 + O_3). \tag{22}$$

The current through open Ca^{2+}-activated K^+ channels is assumed to be ohmic, yielding:

$$I_{K(Ca)} = g_{K(Ca)}(V_m - E_K), \tag{23}$$

in which E_K is the equilibrium potential for the Ca^{2+}-activated K^+ current.

To generate predictions of $I_{K(Ca)}$ in response to voltage-clamp stimuli, we solved numerically the system of seven differential equations ((8), (13), (17)–(21)) with a FORTRAN program, MODDEQ, that uses a Runge–Kutta–Gill method to compute starting values and an Adams–Moulton method for integration. A step size of 10 μs was used; further decreases in step size caused no change in the solution.

Choice of parameter values for modelling $I_{K(Ca)}$

Parameter values related to Ca^{2+}-channel gating were determined directly from measurements of I_{Ca} as described in the Results. We present below a brief description of constraints imposed by experimental data on parameters related to Ca^{2+} regulation. The remaining parameter values were adjusted to provide the best fits to $I_{K(Ca)}$ recorded at potentials between -55 and -30 mV. The final choices of parameter values are listed in Table 2.

Estimation of ξ, *the fractional volume of the submembrane* Ca^{2+} *compartment.* At a membrane potential of -30 mV, the open-state probability of Ca^{2+}-activated K^+ channels in whole-cell recordings is greater than 0·8 (see Results). Single-channel measurements at the same potential suggest that a free $[Ca^{2+}]_i$ in excess of 100 μM is necessary to account for this level of activation (Fig. 13). The chosen value of ξ predicts a steady-state level of 163 μM-Ca_i^{2+} and an open-state probability for the Ca^{2+}-activated K^+ channel of 0·8, using the measured steady-state value of I_{Ca} at -30 mV (data of Fig. 6). Because a lower value of ξ can be offset by assuming a lower Ca^{2+} sensitivity for the K^+ channel, this assignment for ξ is somewhat arbitrary.

Constraint on K_S, *the rate constant for the removal of* Ca^{2+} *from the submembrane compartment.* In response to voltage pulses to values between -50 and -30 mV, whole-cell $I_{K(Ca)}$ reaches a plateau value within several milliseconds. Because $I_{K(Ca)}$

is not fully activated in the steady state at these potentials, particularly at the more negative ones (Fig. 7*B*), $[Ca^{2+}]_i$ must also reach a steady level within several milliseconds; this result places a lower limit of about 400 s^{-1} on the value of K_s.

The authors thank Mr R. A. Jacobs for making excellent experimental apparatus and for preparing the Figures and Drs S. Block, D. P. Corey and R. Horn for providing respectively MODDEQ, data-acquisition, and maximum-likelihood programs. In conjunction with A. J. H., Drs W. M. Roberts and L. Robles W. confirmed the results of the whole-cell recordings described here. Drs M. Cahalan, A. Das, J. Howard, A. V. Maricq, E. Phillips and W. M. Roberts, Ms A. McKenzie and Messrs D. Goldreich and P. Slesinger kindly provided comments on the manuscript. This work was principally supported by National Institutes of Health grant NS22389. The initial experiments, which were conducted at the California Institute of Technology, were supported by a grant from the System Development Foundation and by National Institutes of Health grants NS13154 and GM07737.

REFERENCES

ADAMS, P. R., CONSTANTI, A., BROWN, D. A. & CLARK, R. B. (1982). Intracellular Ca^{2+} activates a fast voltage-sensitive K^+ current in vertebrate sympathetic neurones. *Nature* **296**, 746–749.

AHMED, Z. & CONNOR, J. A. (1979). Measurement of calcium influx under voltage clamp in molluscan neurones using the metallochromic dye Arsenazo III. *Journal of Physiology* **286**, 61–82.

ART, J. J. & FETTIPLACE, R. (1987). Variation of membrane properties in hair cells isolated from the turtle cochlea. *Journal of Physiology* **385**, 207–242.

ART, J. J., FETTIPLACE, R. & FUCHS, P. A. (1984). Synaptic hyperpolarization and inhibition of turtle cochlear hair cells. *Journal of Physiology* **356**, 525–550.

ASHMORE, J. F. (1983). Frequency tuning in a frog vestibular organ. *Nature* **304**, 536–538.

ASHMORE, J. F. & ATTWELL, D. (1985). Models for electrical tuning in hair cells. *Proceedings of the Royal Society* B **226**, 325–344.

ASHMORE, J. F. & MEECH, R. W. (1986). Ionic basis of membrane potential in outer hair cells of guinea pig cochlea. *Nature* **322**, 368–371.

BARISH, M. E. & THOMPSON, S. H. (1983). Calcium buffering and slow recovery kinetics of calcium-dependent outward current in molluscan neurones. *Journal of Physiology* **337**, 201–219.

BARRETT, J. N., MAGLEBY, K. L. & PALLOTTA, B. S. (1982). Properties of single calcium-activated potassium channels in cultured rat muscle. *Journal of Physiology* **331**, 211–230.

BERS, D. M. (1982). A simple method for the accurate determination of free [Ca] in Ca-EGTA solutions. *American Journal of Physiology* **242**, C404–408.

BROWN, D. A., CONSTANTI, A. & ADAMS, P. R. (1983). Ca-activated potassium current in vertebrate sympathetic neurones. *Cell Calcium* **4**, 407–420.

BYERLY, L. & HAGIWARA, S. (1982). Calcium currents in internally perfused nerve cell bodies of *Limnea stagnalis*. *Journal of Physiology* **322**, 503–528.

BYERLY, L. & YAZEJIAN, B. (1986). Intracellular factors for the maintenance of calcium currents in perfused neurones from the snail, *Lymnaea stagnalis*. *Journal of Physiology* **370**, 631–650.

COLQUHOUN, D. & SIGWORTH, F. J. (1983). Fitting and statistical analysis of single-channel records. In *Single-Channel Recording*, ed. SAKMANN, B. & NEHER, E., pp. 191–263. New York: Plenum.

CONNOR, J. A. (1978). Slow repetitive activity from fast conductance changes in neurons. *Federation Proceedings* **37**, 2139–2145.

CONNOR, J. A. & STEVENS, C. F. (1971). Voltage clamp studies of a transient outward membrane current in gastropod neural somata. *Journal of Physiology* **213**, 21–30.

COREY, D. P., DUBINSKY, J. M. & SCHWARTZ, E. A. (1984). The calcium current in inner segments of rods from the salamander (*Ambystoma tigrinum*) retina. *Journal of Physiology* **354**, 557–575.

COREY, D. P. & HUDSPETH, A. J. (1979). Ionic basis of the receptor potential in a vertebrate hair cell. *Nature* **281**, 675–677.

CRAWFORD, A. C. & FETTIPLACE, R. (1980). The frequency selectivity of auditory nerve fibres and hair cells in the cochlea of the turtle. *Journal of Physiology* **306**, 79–125.

CRAWFORD, A. C. & FETTIPLACE, R. (1981). An electrical tuning mechanism in turtle cochlear hair cells. *Journal of Physiology* **312**, 377–412.

DUBINSKY, J. M. & OXFORD, G. S. (1984). Ionic currents in two strains of rat anterior pituitary tumor cells. *Journal of General Physiology* **83**, 309–339.

FENWICK, E. M., MARTY, A. & NEHER, E. (1982). Sodium and calcium channels in bovine chromaffin cells. *Journal of Physiology* **331**, 599–635.

FERNANDEZ, J. M., FOX, A. P. & KRASNE, S. (1984). Membrane patches and whole-cell membranes: a comparison of electrical properties in rat clonal pituitary (GH3) cells. *Journal of Physiology* **356**, 565–585.

FURUKAWA, T. & MATSUURA, S. (1978). Adaptive rundown of excitatory post-synaptic potentials at synapses between hair cells and eighth nerve fibres in the goldfish. *Journal of Physiology* **276**, 193–209.

GORMAN, A. L. F., LEVY, S., NASI, E. & TILLOTSON, D. (1984). Intracellular calcium measured with calcium-sensitive micro-electrodes and Arsenazo III in voltage-clamped *Aplysia* neurones. *Journal of Physiology* **353**, 127–142.

GORMAN, A. L. F. & THOMAS, M. V. (1980). Potassium conductance and internal calcium accumulation in a molluscan neurone. *Journal of Physiology* **308**, 287–313.

HAGIWARA, S. & OHMORI, H. (1982). Studies of calcium channels in rat clonal pituitary cells with patch electrode voltage clamp. *Journal of Physiology* **331**, 231–252.

HAMILL, O. P., MARTY, A., NEHER, E., SAKMANN, B. & SIGWORTH, F. J. (1981). Improved patch-clamp techniques for high-resolution current recording from cells and cell-free membrane patches. *Pflügers Archiv* **391**, 85–100.

HILLE, B., WOODHULL, A. M. & SHAPIRO, B. I. (1975). Negative surface charge near sodium channels of nerve: divalent ions, monovalent ions, and pH. *Philosophical Transactions of the Royal Society* B **270**, 301–318.

HODGKIN, A. L. & HUXLEY, A. F. (1952). A quantitative description of membrane current and its application to conduction and excitation in nerve. *Journal of Physiology* **117**, 500–544.

HODGKIN, A. L. & KATZ, B. (1949). The effect of sodium ions on the electrical activity of the giant axon of the squid. *Journal of Physiology* **108**, 37–77.

HODGKIN, A. L. & KEYNES, R. D. (1957). Movements of labelled calcium in squid giant axons. *Journal of Physiology* **138**, 253–281.

HUDSPETH, A. J. (1983). Mechanoelectrical transduction by hair cells in the acousticolateralis sensory system. *Annual Review of Neuroscience* **6**, 187–215.

HUDSPETH, A. J. (1985). The cellular basis of hearing: the biophysics of hair cells. *Science* **230**, 745–752.

HUDSPETH, A. J. (1986). The ionic channels of a vertebrate hair cell. *Hearing Research* **22**, 21–27.

HUDSPETH, A. J. & LEWIS, R. S. (1988). A model for electrical resonance and frequency tuning in saccular hair cells of the bull-frog, *Rana catesbeiana*. *Journal of Physiology* **400**, 275–297.

LATORRE, R. & MILLER, C. (1983). Conduction and selectivity in potassium channels. *Journal of Membrane Biology* **71**, 11–30.

LEWIS, R. S. (1984*a*). A biophysical model for electrical resonance in hair cells of the bullfrog's sacculus. *Society for Neuroscience Abstracts* **10**, 11.

LEWIS, R. S. (1984*b*). The ionic basis of frequency selectivity in hair cells of the bullfrog's sacculus. Ph.D. Dissertation, California Institute of Technology, Pasadena, CA, U.S.A.

LEWIS, R. S. & HUDSPETH, A. J. (1983*a*). Frequency tuning and ionic conductances in hair cells of the bullfrog's sacculus. In *Hearing – Physiological Bases and Psychophysics*, ed. KLINKE, R. & HARTMANN, R., pp. 17–24. Berlin: Springer-Verlag.

LEWIS, R. S. & HUDSPETH, A. J. (1983*b*). Voltage- and ion-dependent conductances in solitary vertebrate hair cells. *Nature* **304**, 538–541.

MAGLEBY, K. L. & PALLOTTA, B. S. (1983). Calcium dependence of open and shut interval distributions from calcium-activated potassium channels in cultured rat muscle. *Journal of Physiology* **344**, 585–604.

MARTY, A. & NEHER, E. (1983). Tight-seal whole-cell recording. In *Single-Channel Recording*, ed. SAKMANN, B. & NEHER, E., pp. 107–122. New York: Plenum.

MARTY, A. & NEHER, E. (1985). Potassium channels in cultured bovine adrenal chromaffin cells. *Journal of Physiology* **367**, 117–141.

MEECH, R. W. & STANDEN, N. B. (1985). Potassium activation in *Helix aspersa* neurones under voltage clamp: a component mediated by calcium influx. *Journal of Physiology* **249**, 211–239.

MOCZYDLOWSKI, E. & LATORRE, R. (1983). Gating kinetics of Ca^{2+}-activated K^+ channels from rat muscle incorporated into planar lipid bilayers. *Journal of General Physiology* **82**, 511–542.

MOOLENAAR, W. H. & SPECTOR, I. (1979). The calcium current and the activation of a slow potassium conductance in voltage-clamped mouse neuroblastoma cells. *Journal of Physiology* **292**, 307–323.

NEHER, E. (1971). Two fast transient current components during voltage clamp on snail neurons. *Journal of General Physiology* **58**, 36–53.

OHMORI, H. (1984). Studies of ionic currents in the isolated vestibular hair cell of the chick. *Journal of Physiology* **350**, 561–581.

PALLOTTA, B. S., HEPLER, J. R., OGLESBY, S. A. & HARDEN, T. K. (1987). A comparison of calcium-activated potassium channel currents in cell-attached and excised patches. *Journal of General Physiology* **89**, 985–997.

ROBERTS, W. M., ROBLES, L. & HUDSPETH, A. J. (1986). Correlation between the kinetic properties of ionic channels and the frequency of membrane-potential resonance in hair cells of the bullfrog. In *Auditory Frequency Selectivity*, ed. MOORE, B. C. J. & PATTERSON, R. D., pp. 89–95. New York: Plenum.

SAND, O., OZAWA, S. & HAGIWARA, S. (1975). Electrical and mechanical stimulation of hair cells in the mudpuppy. *Journal of Comparative Physiology* **102**, 13–26.

SEWELL, W. F. (1984). The effects of furosemide on the endocochlear potential and auditory-nerve fiber tuning curves in cats. *Hearing Research* **14**, 305–314.

SIGWORTH, F. J. (1980). The variance of sodium current fluctuations at the node of Ranvier. *Journal of Physiology* **307**, 97–129.

SMITH, S. J. (1978). The mechanism of bursting pacemaker activity in neurons of the mollusc *Tritonia diomedia*. Ph.D. Dissertation, University of Washington, Seattle, WA, U.S.A.

SMITH, S. J., MACDERMOTT, A. B. & WEIGHT, F. F. (1983). Detection of intracellular Ca^{2+} transients in sympathetic neurones using arsenazo III. *Nature* **304**, 350–352.

SMITH, S. J. & ZUCKER, R. S. (1980). Aequorin response facilitation and intracellular calcium accumulation in molluscan neurones. *Journal of Physiology* **300**, 167–196.

STANDEN, N. B. & STANFIELD, P. R. (1982). A binding-site model for calcium channel inactivation that depends on calcium entry. *Proceedings of the Royal Society* B **217**, 101–110.

SULLIVAN, W. E. & KONISHI, M. (1984). Segregation of stimulus phase and intensity coding in the cochlear nucleus of the barn owl. *Journal of Neuroscience* **4**, 1787–1799.

YELLEN, G. (1982). Single Ca^{2+}-activated nonselective cation channels in neuroblastoma. *Nature* **296**, 357–359.